Mechanistic basis of gene regulation by SRCAP and H2A.Z

Armelle Tollenaere[1*], Enes Ugur[2,3], Cédric Deluz[1], Heinrich Leonhardt[3], David M Suter[1*]

[1]Ecole Polytechnique Fédérale de Lausanne, School of Life Sciences, Institute of Bioengineering, Lausanne, Switzerland
[2]Department of Proteomics and Signal Transduction, Max-Planck Institute of Biochemistry, Martinsried 82152, Germany.
[3]Faculty of Biology and Center for Molecular Biosystems (BioSysM), Human Biology and BioImaging, Ludwig-Maximilians-Universität München, Munich 81377, Germany.

*Correspondence: armelle.tollenaere@epfl.ch (A.T.) and david.suter@epfl.ch (D.S)

Summary

A central problem in gene regulation is to discriminate gene regulatory functions of chromatin composition from the one of chromatin-modifying complexes. This question has been virtually unexplored in the context of the H2A.Z histone variant and its incorporation into nucleosomes by the Snf2 Related CREBBP Activator Protein (SRCAP) complex. Here we combine rapid SRCAP depletion, a SRCAP mutant lacking H2A.Z deposition activity, and quantitative genome-wide approaches to dissect how SRCAP and H2A.Z regulate transcription in pluripotent stem cells. We find that SRCAP exhibits essential H2A.Z-independent functions in preventing DNA binding of lineage-specific transcription factors at enhancers and stimulating transcription factor binding at promoters. In contrast, H2A.Z acts mainly as a transcriptional repressor that requires dynamic reloading by SRCAP throughout the cell cycle. Our study demonstrates how the SRCAP-H2A.Z axis broadly orchestrates transcription to promote self-renewal, inhibit differentiation, and maintain plasticity of pluripotent stem cells.

Introduction

In Eukaryotes, most DNA is wrapped around nucleosomes made of histone octamers. While two copies of the four canonical histones make up most nucleosomes, histone variants can replace them in specific positions of the genome. H2A.Z is a highly conserved H2A histone variant essential for zygotic genome activation in drosophila and zebrafish and for post-implantation development in the mouse[1–3]. In vertebrates, there are two different isoforms of H2A.Z (H2A.Z.1 and H2A.Z.2) that differ by only 3 amino acids[4]. H2A.Z plays a central role in self-renewal and lineage commitment of multiple types of stem cells, including mouse pluripotent stem cells (PSCs)[5–7]. Both Snf2 Related CREBBP Activator Protein (SRCAP) and

Tip60/p400 remodeler complexes ensure H2A.Z deposition in mammals[8,9]. In mouse PSCs, H2A.Z deposition is mainly achieved by the SRCAP complex, made of the SRCAP protein bearing the catalytic ATPase activity and 9 other subunits[10]. The SRCAP complex binds to canonical nucleosomes and swaps the H2A-H2B dimer with a H2A.Z-H2B dimer[8]. The SRCAP complex was also reported to facilitate the recruitment of some transcriptional regulators, but whether this function is independent of its role in depositing H2A.Z is unclear[11–13].

In PSCs, H2A.Z is broadly enriched at active and bivalent/poised promoters and enhancers[14,15]. H2A.Z has been proposed to regulate transcription at multiple levels, i.e. by modulating chromatin accessibility, repressing DNA methylation, altering transcription factor (TF) binding and enhancing RNA Polymerase II pausing[16–20]. MNase-ChIP assays and Cryo-EM studies reported that H2A.Z nucleosomes protect shorter segments of DNA compared to canonical nucleosomes, which was suggested to cause nucleosome destabilization and facilitate protein-DNA interactions[21].

Our mechanistic understanding of transcriptional regulation by SRCAP and H2A.Z remains obscured by conflicting evidence and technical challenges. First, studies on the role of H2A.Z in regulating chromatin accessibility and TF binding report opposite effects[5,16,18,22,23]. Second, whether H2A.Z-containing nucleosomes are evicted or replaced with canonical nucleosomes in studies depleting H2A.Z is unclear[5,24,25,20]. Thus, the specific function of H2A.Z with respect to H2A has not yet been addressed in vivo. Third, the proposed role of H2A.Z in inhibiting DNA methylation in mammals is supported by either correlative evidence, or by slow H2A.Z knockdown approaches that may reflect indirect effects of H2A.Z loss[26,27]. It thus remains unclear whether H2A.Z plays a direct role in regulating DNA methylation in mammals. Fourth, depletion of H2A.Z results in genome-wide redistribution of the yeast SRCAP homolog (SWR1)[28], and nucleosomal H2A.Z inhibits the binding of human SRCAP[23]. Given the potential H2A.Z-independent role of SRCAP in recruiting transcriptional regulators[29], the perturbation of SRCAP recruitment triggered by H2A.Z knockdown may lead to H2A.Z-independent consequences on gene regulation.

Here we combine rapid depletion of SRCAP, a broad range of genomic and proteomic approaches and a catalytically-dead SRCAP mutant. This allows us to dissect the direct and acute consequences of SRCAP loss and to uncouple H2A.Z deposition from other SRCAP functions in transcriptional regulation. Our study reveals how SRCAP and H2A.Z coordinate their distinct functions to orchestrate gene regulation governing self-renewal and plasticity.

Results

Dynamic and cell cycle-dependent SRCAP-mediated H2A.Z positioning

To study the dynamics of H2A/H2A.Z exchange by SRCAP, we generated a CGR8 mouse embryonic stem cell (mESC) line that allows rapid degradation of the catalytic subunit of the SRCAP complex (SRCAP), using the auxin-inducible protein degradation system[30]. We knocked-in a YPet-AID (YA) sequence into the 3'end of both alleles of the *srcap* gene and stably expressed the OsTir1 receptor by lentiviral transduction to generate the SRCAP-Ypet-AID Tir1 (SYAT) cell line. We validated the pluripotency of SYAT cells by Alkaline Phosphatase assay and RT-QPCR of pluripotency transcription factors (Figure S1A). SRCAP-YA was localized in the nucleus in interphase and colocalized with condensed chromosomes during mitosis (Figure S1B), as reported before[31]. CUT&Tag analysis revealed that SRCAP-YA was enriched at promoters and preferentially colocalized with active transcription start sites (TSS) and H2A.Z peaks (Figure S1C and 1A), in line with enrichment of SWR1 at promoters of active genes in yeast[28]. Upon addition of the auxin hormone indole-3-acetic acid (IAA), SRCAP-YA was rapidly depleted both in interphase and mitotic cells (Figure 1B), accompanied by a decreased association of H2A.Z with mitotic chromosomes (Figure S1D).

We then quantified the genome-wide impact of SRCAP loss on H2A.Z and H2A positioning by ChIP-seq at 2, 4, 6 or 8 hours (h) after IAA addition. We observed rapid depletion of H2A.Z and filling of the corresponding regions with H2A, as expected from the function of SRCAP in exchanging H2A for H2A.Z (Figure 1C and D). H2A.Z was lost and replaced by H2A at 98% of H2A.Z ChIP-seq peaks with the majority of peaks (72%) losing most H2A.Z within 2 h (Figure S1E). We then identified regions specifically enriched for the H2A.Z.1 or H2A.Z.2 isoforms using data from Mylonas et al.[20], and found no difference in H2A.Z turnover at these regions, suggesting that H2A.Z.1 and H2A.Z.2 are similarly affected by SRCAP depletion (Figure S1F). The rate of SRCAP-mediated H2A.Z exchange was the highest at active promoters, followed by active enhancers, and slightly slower at bivalent and poised enhancers (Figure 1E and F). The pace of H2A.Z loss was particularly fast at nucleosomes surrounding TSS of active genes (Figure 1G) and scaled with transcriptional activity of the corresponding genes (Figure S1G). Loci with the highest H2A.Z turnover were characterized by the highest SRCAP levels, as well as higher enrichment of the chromatin remodelers SWI/SNF, NuRD and Ep400 and of several PSC transcription factors (TFs) (Figure 1H and S1H), suggesting their potential role in evicting H2A.Z nucleosomes. Since the pioneer TFs (pTFs) OCT4 and SOX2 play a central role in maintaining chromatin accessibility in PSCs[32,33], we next examined H2A.Z co-localization with regions that depend on OCT4 and SOX2 for chromatin accessibility maintenance[32,33]. We found that H2A.Z was rapidly lost in these regions upon depletion of SRCAP (Figure S1I). Furthermore, knockdown of OCT4 using the Tet-off ZHBTc4 cell line[34] (see methods) resulted in restoration of H2A.Z occupancy (Figure S1J), suggesting that OCT4 mediates H2A.Z

eviction. Taken together, these findings are in line with H2A.Z nucleosome eviction by the transcriptional machinery and gene regulatory factors[35,36].

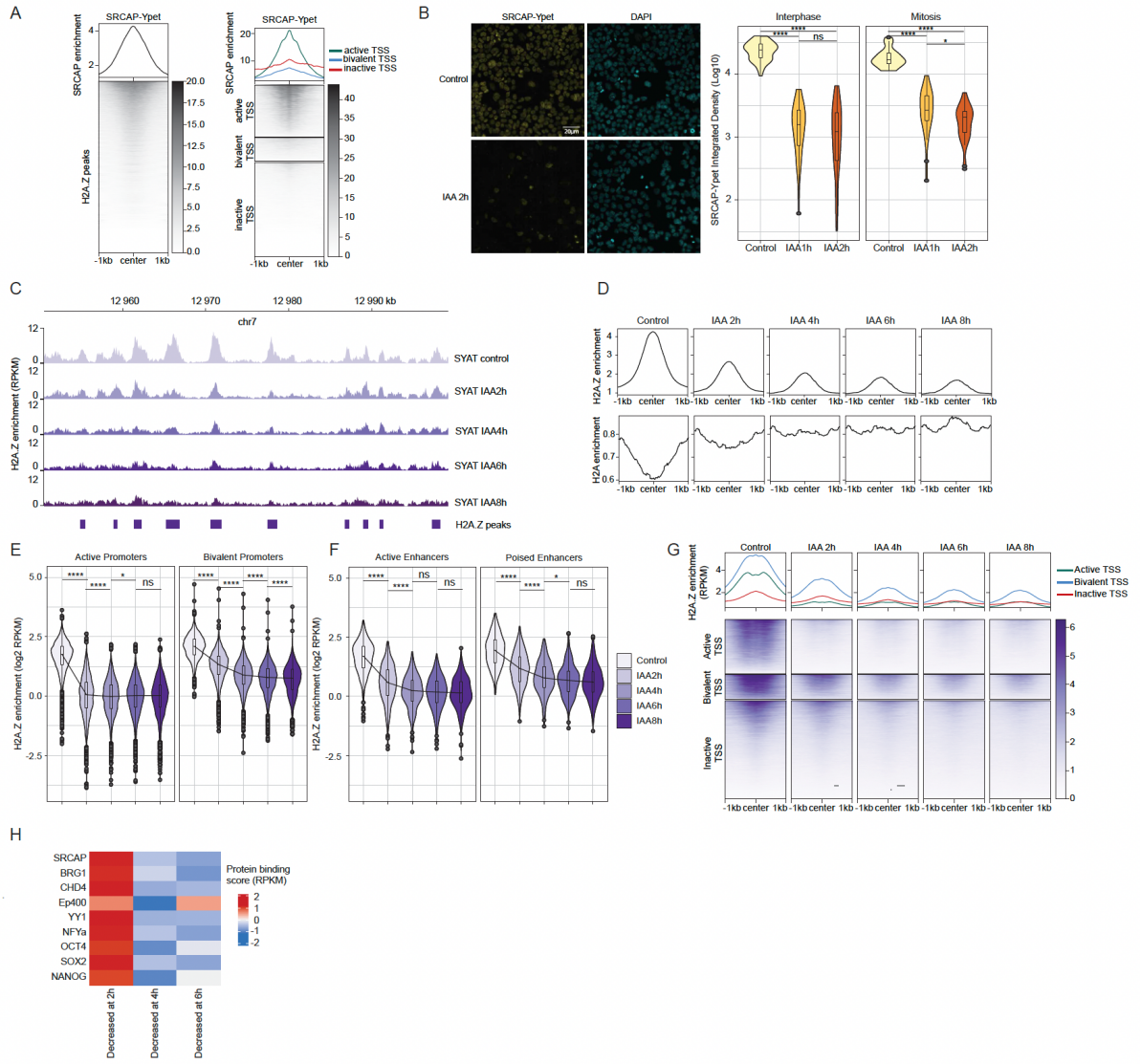

Figure 1. SRCAP degradation leads to rapid replacement of H2A.Z by H2A. (A) SRCAP-YPet-AID genomic mapping by CUT&Tag. (B) Left panel: Microscopy snapshots of SYAT cells, treated with IAA or control for 2 h and stained with DAPI. Right panel: Quantification of total SRCAP-YA signal in interphase and mitotic cells treated with IAA or control. N = 50 cells per condition. C. Genome tracks of H2A.Z ChIP-Seq in SYAT cells treated with IAA. (D) ChIP-Seq profiles of H2A.Z and H2A in SYAT cells treated with IAA. (E) and (F). H2A.Z enrichment at active and bivalent promoters (E) and enhancers (F) upon SRCAP degradation. Black line: changes in median values. Boxes: interquartile range; dots: outlier points. (G) ChIP-seq metaplots and heatmaps of H2A.Z enrichment around the TSS of active, bivalent, and inactive genes. (H) Z-score enrichment of different DNA-binding proteins for the different H2A.Z turnover groups. p-values were determined by a pairwise Wilcoxon test, *: p<0.05, **: p<0.01, ***: p<0.001, ****: p<0.0001, ns: non-significant.

As TF binding, chromatin remodeler activity and transcription activity vary across the cell cycle, we next determined H2A.Z positioning in different cell cycle phases. To do so, we used PSCs

expressing YPet fused to a mitotic degron (MD), allowing to sort cells in early G1 (EG1), late G1 (LG1), S or G2/M phases after Hoechst DNA staining[33]. We also used a mitotic cell purification approach without drug-mediated cell cycle synchronization, as described in [37]. We then used calibrated ChIP-seq (see Methods) to dissect how H2A.Z occupancy changes during the cell cycle. Global variations of H2A.Z through the cell cycle were modest (Figure 2A) and H2A.Z was mostly located at active and bivalent/poised regulatory elements (Figure 2B). In line with transcription-dependent H2A.Z eviction, H2A.Z was lost at active promoters and enhancers at the mitosis to EG1 transition, but accumulated at bivalent and poised enhancers (Figure S2A-B). We neither observed a mitotic shift of H2A.Z on the TSS as reported in bladder cancer cells[38], nor a mitotic H2A.Z depletion at promoters as reported in trophoblast cells[39], suggesting that the mitotic H2A.Z landscape is cell type-specific. We then classified promoters and enhancers according to changes in H2A.Z occupancy between G2 phase and mitosis (Figure 2C and S2C). Global H2A.Z levels were equalized during mitosis at promoters and enhancers, in line with a locus-independent, quantitative resetting of the H2A.Z landscape across the genome before cells divide and enter the next cell cycle (Figure 2D and S2D).

Promoters in cluster 1 (decreased H2A.Z mitotic levels) showed enrichment for Gene Ontology (GO) terms associated with lineage specification, while promoters in cluster 3 (increased H2A.Z mitotic levels) were enriched in genes related to general cellular functions (Figure S2E). In interphase, cluster 3 promoters had lower H2A.Z levels than cluster 1 and 2 promoters. The average expression levels of genes downstream of these promoters were similar across all clusters, although highly-expressed genes were more enriched in cluster 3 (Figure 2E). In the three enhancer clusters, both the expression level of genes regulated by these enhancers and enhancer RNA levels were comparable (Figure S2F). Next, we performed ChIP-seq in asynchronous and mitotic cells on the acetylated form of H2A.Z (acH2A.Z), which is associated with active regulatory elements and is positively correlated with transcription levels[40]. In contrast to total H2A.Z, mitotic acH2A.Z levels were decreased genome-wide and in all three mitotic clusters (Figure 2F and S2G, S2H), reflecting a shift in the equilibrium between acetylation and deacetylation during mitosis.

The mitotic chromosome colocalization of SRCAP[31] and the preservation of H2A.Z content on active promoters during mitosis prompted us to investigate SRCAP-dependent H2A.Z positioning during mitosis. To do so, we treated cells with IAA for 1 h and sorted mitotic cells, thus selecting cells having undergone SRCAP depletion around the G2-M transition. We also collected asynchronous cells after this 1 h treatment for comparison. Remarkably, 1 h IAA treatment was sufficient to decrease H2A.Z occupancy genome-wide (Figure 2G and S2I), at bivalent/poised promoters and enhancers in mitosis but not in interphase (Figure 2H and S2J). In contrast, 1 h IAA treatment in both mitosis and interphase decreased H2A.Z levels at active promoters and enhancers, in line with their particularly high H2A.Z turnover rate (Figure 2H

and S2J). Taken together, this suggests that SRCAP-mediated H2A.Z deposition and eviction are even more dynamic in mitosis than interphase, despite the very low transcriptional activity of mitotic cells[41], pointing at a transcription-independent mechanism of mitotic H2A.Z eviction.

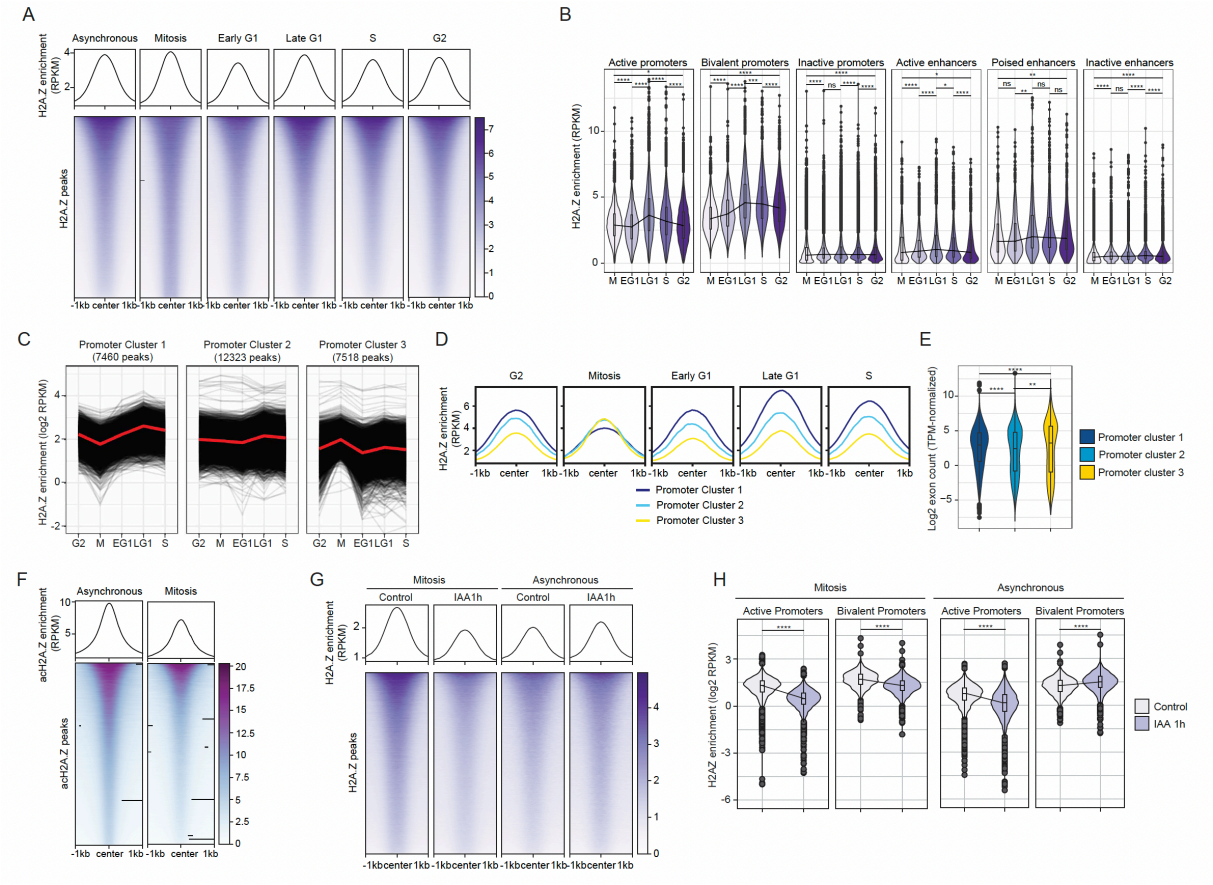

Figure 2. H2A.Z deposition across the cell cycle. (A) Heatmaps and metaplots of H2A.Z enrichment centered on the summit of H2A.Z peaks across the cell cycle. (B) H2A.Z enrichment across the cell cycle in promoters or enhancers, classified according to their activity. (C) H2A.Z enrichment in promoter peaks with decreased, stable or increased H2A.Z levels with respect to G2 and EG1 phases. (D) H2A.Z enrichment around H2A.Z peaks in the clusters shown in (C) Intronic counts of genes downstream to each cluster defined in (C) in wt ESC. (F) Heatmaps and metaplots of acH2A.Z enrichment centered on the summit of acH2A.Z peaks in asynchronous versus mitotic cells. (G) Heatmap of H2A.Z enrichment centered on the summit of H2A.Z peaks in mitotic or asynchronous SYAT cells treated for 1 h with IAA. (H) H2A.Z enrichment in promoters of mitotic or asynchronous SYAT cells treated for 1 h with IAA. p-values were determined by a pairwise Wilcoxon test, ****: $p<0.0001$, *: $p<0.05$, ns: non-significant.

SRCAP depletion unleashes the expression of master regulators of cell fate

As H2A.Z knockdown was previously shown to induce transcriptional deregulation in PSCs[42], we then quantified the impact of acute depletion of SRCAP on transcription by treating SYAT cells with IAA for 2, 4, 6 or 8 h followed by nuclear RNA-seq. In parallel, we also treated wt CGR8 cells with IAA for 4 h to account for unspecific effects of IAA. We quantified both intronic reads, which have been shown to accurately reflect acute transcriptional activity[43], and exonic reads. In wt CGR8 cells, 4 h of IAA treatment did not impact transcription (Figure S3A). In SYAT cells, changes in intronic reads were already apparent after 2 h and peaked after 6 h of

IAA treatment, when an approximately equal number of genes were up- (211) and downregulated (276) (Figure 3A and Table S1). Mature transcripts were more gradually affected starting from 2 h of IAA treatment (Figure S3B). These results differ from those reported using H2A.Z knockdown in mESCs, which mainly identified upregulated genes[20,42] that poorly overlap with the genes we identified (Figure S3C). This suggests that SRCAP and H2A.Z may have distinct roles in transcriptional regulation. While up- and downregulated genes displayed higher initial H2A.Z levels at their promoters, the pace of H2A.Z removal was comparable between transcriptionally-affected and unaffected genes (Figure S3D). We then focused specifically on bivalent genes, which are poised to be activated during early differentiation and many of which play an important role in early embryonic development[44]. Bivalent genes were markedly over-represented among upregulated genes, suggesting that SRCAP depletion unleashes their expression (Figure 3B). While no clear functional gene category was overrepresented in downregulated genes (Figure S3E), upregulated genes were highly enriched in DNA-binding proteins and in particular in lineage-specific transcription factors (Figure 3C and S3F). Among those were TFs associated with differentiation towards all three germ layers, especially TFs involved in mesoderm differentiation (Gata3, Gata6, BMP4, Meis1, Lefty2) but also TFs associated with pluripotency maintenance (Nanog, Myc, Trim28, Zfp42) (Figure S3G, Table S1). In contrast, downregulated genes were enriched in ubiquitously expressed genes (Figure 3D). As lineage-specific genes tend to be regulated in an enhancer-dependent manner[45], we quantified the number of promoter-enhancer loops formed for each gene (see Methods). On average, upregulated genes tended to form a higher number of promoter-enhancer loops than downregulated genes (Figure 3E). We then verified whether transcriptional changes triggered by SRCAP depletion were accompanied by changes in the proteome of the IAA-treated cells as quantified by Mass Spectrometry (see Methods). After 4 h of IAA treatment, only 52 and 30 proteins were significantly increased and decreased in their levels, respectively, with SRCAP being the most significantly downregulated protein (Figure 3F, Table S2). GO terms associated with DNA binding and transcriptional regulation were enriched in upregulated proteins (Figure S3H), in line with upregulated genes at the mRNA level.

As SRCAP degradation in mitosis led to a strong loss of H2A.Z from chromatin, we then investigated the impact of mitotic SRCAP depletion on gene reactivation during early G1 phase. To allow isolation of cells during mitotic exit, we generated a SYAT cell line expressing mCherry fused to a mitotic degron (MD). We treated SYAT/mCherry-MD cells with IAA for 1 h, followed by sorting of EG1 cells (undergoing SRCAP depletion during mitosis) or LG1 cells (undergoing SRCAP depletion during G1). Since transcriptional changes after such a short IAA treatment were modest, we used .25 log2 fold-change as a threshold to quantify up- and downregulated genes in these conditions. Mitotic SRCAP depletion resulted mainly in gene

downregulation in EG1 (Figure 3G), many of which were housekeeping genes (Figure S3I). In contrast, SRCAP depletion during G1 resulted in a smaller number of downregulated genes (Figure 3H). This suggests that SRCAP activity during mitosis and at mitotic exit is mainly required for transcriptional reactivation in early G1.

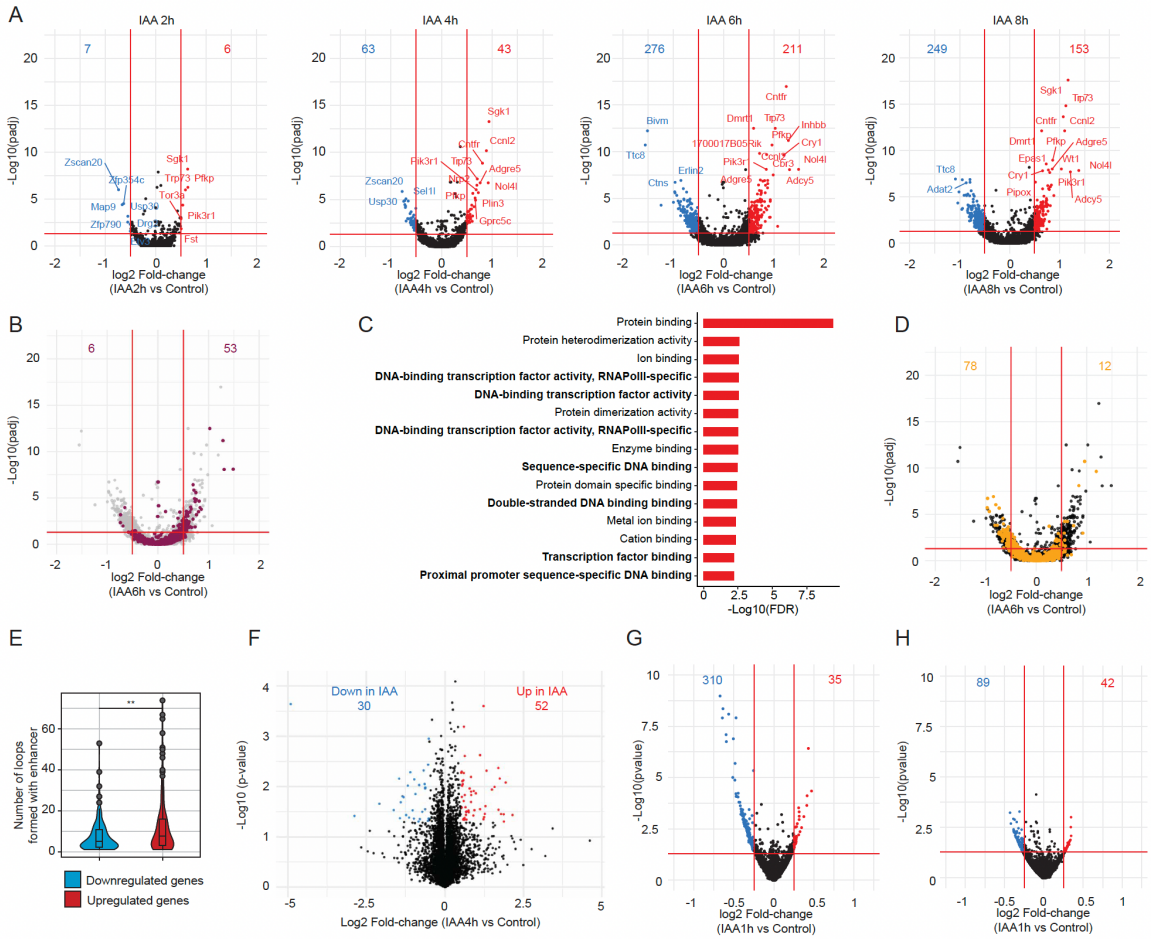

Figure 3. SRCAP degradation leads to transcriptional deregulation. (A) Fold-change of intronic reads and adjusted p-value for SYAT cells treated for 2, 4, 6 and 8 h with IAA. Numbers: genes significantly downregulated (blue) or upregulated (red) with a threshold of |log2FC|>0.5 and adjusted p-value < 0.05. (B) Fold-change of intronic reads and adjusted p-value for SYAT cells treated for 6 h with IAA. Genes regulated by a bivalent promoter are colored. (C) Top 15 GO terms enriched for genes upregulated at 6 h with the category “molecular function”. (D) Fold-change of intronic reads and adjusted p-value for SYAT cells treated for 6 h with IAA. Ubiquitously-expressed genes are colored. (E) Number of promoter-enhancer loops formed for genes found to be downregulated or upregulated at any time point. p-values were determined by a pairwise Wilcoxon test, **: p<0.01. (F) Changes in proteome composition in SYAT cells treated with IAA for 4 h compared to control. Numbers: proteins enriched (blue) or depleted (red) from the proteome upon IAA treatment with a threshold of |log2FC|>0.5 and p-value < 0.05. (G) and (H) Fold-change of intronic reads, for SYAT cells treated for 1 h with IAA and sorted in EG1 (G) or LG1 (H). Numbers: genes significantly downregulated (blue) or upregulated (red) with a threshold of |log2FC|>0.25 and p-value < 0.05.

SRCAP depletion alters histone modifications and nucleosome properties

To understand the mechanisms underlying changes in transcriptional activity upon SRCAP depletion, we next analyzed changes in histone post-translational modifications and

nucleosome properties. We first performed ChIP-seq for the active H3K4me3 and the repressive H3K27me3 and H2AK119ub1 marks in SYAT cells treated with IAA or control for 4, 6 and 8 h. After 4 h of IAA treatment, H3K4me3 levels rapidly decreased in 66.6% of H3K4me3-enriched regions, with a marked decrease at bivalent promoters, while they increased (4.4%) or remained stable (29%) in a smaller fraction of regions (Figure 4A-B and S4A). This is in line with the role of H2A.Z in recruiting SET1/COMPASS complexes[5], which allows H3K4me3 maintenance[46]. Changes in H3K4me3 enrichment at +1 nucleosomes were mildly correlated with transcriptional changes for both active and bivalent genes (Figure 4C and S4B), and promoters of downregulated genes displayed a more pronounced and continuous decrease of H3K4me3 (Figure S4C). Taken together, H3K4me3 changes upon SRCAP depletion are in line with the role of H3K4me3 in fostering transcriptional activity[47,48].
H3K27me3 levels decreased at 27.6% of regions (4799 peaks) but also increased at 19.6% of regions (3402 peaks), including those located at bivalent promoters (Figure 4A, D and S4D). Conversely, H2AK119ub1 displayed a massive increase at most enriched loci (52.6%, 20881 peaks), especially at bivalent promoters (Figure 4A, E and S4E). In contrast to downregulated genes, upregulated genes showed high initial levels of H3K27me3, H2AK119Ub1 and H3K4me3, in line with the upregulation of bivalent genes (Figure S4C, F and G). Therefore, despite the repressive nature of histone mark changes at bivalent promoters, these genes were transcriptionally upregulated. This indicates that these marks play little, if any, instructive role in the direct transcriptional perturbations observed at bivalent genes upon SRCAP depletion.
We next performed MNase-seq to analyze the impact of SRCAP/H2A.Z loss on individual nucleosomes. We used two different concentrations of MNase (hereafter referred to as high and low, see Methods) on SYAT cells treated with control or IAA for 4 h. To study the influence of H2A.Z on nucleosome properties in the context of chromatin, we classified nucleosomes detected in MNase-Seq in four classes according to H2A.Z enrichment scores. At both promoters and enhancers, H2A.Z enrichment scaled with nucleosome occupancy (Figure 4F and S4H). However, this coupling was also observed upon SRCAP/H2A.Z depletion, suggesting that nucleosome occupancy is not primarily regulated by H2A.Z but is mostly dependent on the genomic context. The size of nucleosome-protected fragments increased upon SRCAP degradation independently of initial H2A.Z levels in regions containing these nucleosomes (Figure 4G and S4I). While this is in agreement with the reported unwrapped state of H2A.Z nucleosomes[21], this also raises the possibility that SRCAP itself could unwrap nucleosomes independently of H2A.Z deposition, in line with the ability of SWR1 to unwrap nucleosomes in vitro[49,50]. We then focused on fragile nucleosomes, which are defined by a high signal ratio between MN-low versus MN-high digestion and are enriched around TSS and TF binding sites[51,52]. Nucleosome fragility scaled with H2A.Z levels at active and bivalent

regulatory regions (Figure 4H and S4J), in agreement with studies reporting H2A.Z enrichment in fragile nucleosomes[53–55]. Surprisingly, IAA treatment did not induce a global decrease of nucleosome fragility (Figure 4H and S4J). Furthermore, nucleosome fragility was unchanged and increased at +1 nucleosomes of downregulated and upregulated genes, respectively (Figure S4K). This suggests that H2A.Z nucleosomes are not intrinsically more fragile than canonical nucleosomes, but that fragility depends mainly on the genomic context. This also implies that transcriptional changes upon SRCAP depletion cannot be explained by a general alteration of nucleosome properties caused by the replacement of H2A.Z with H2A, and that changes in +1 nucleosome fragility are most likely a consequence rather than a cause of changes in transcriptional activity.

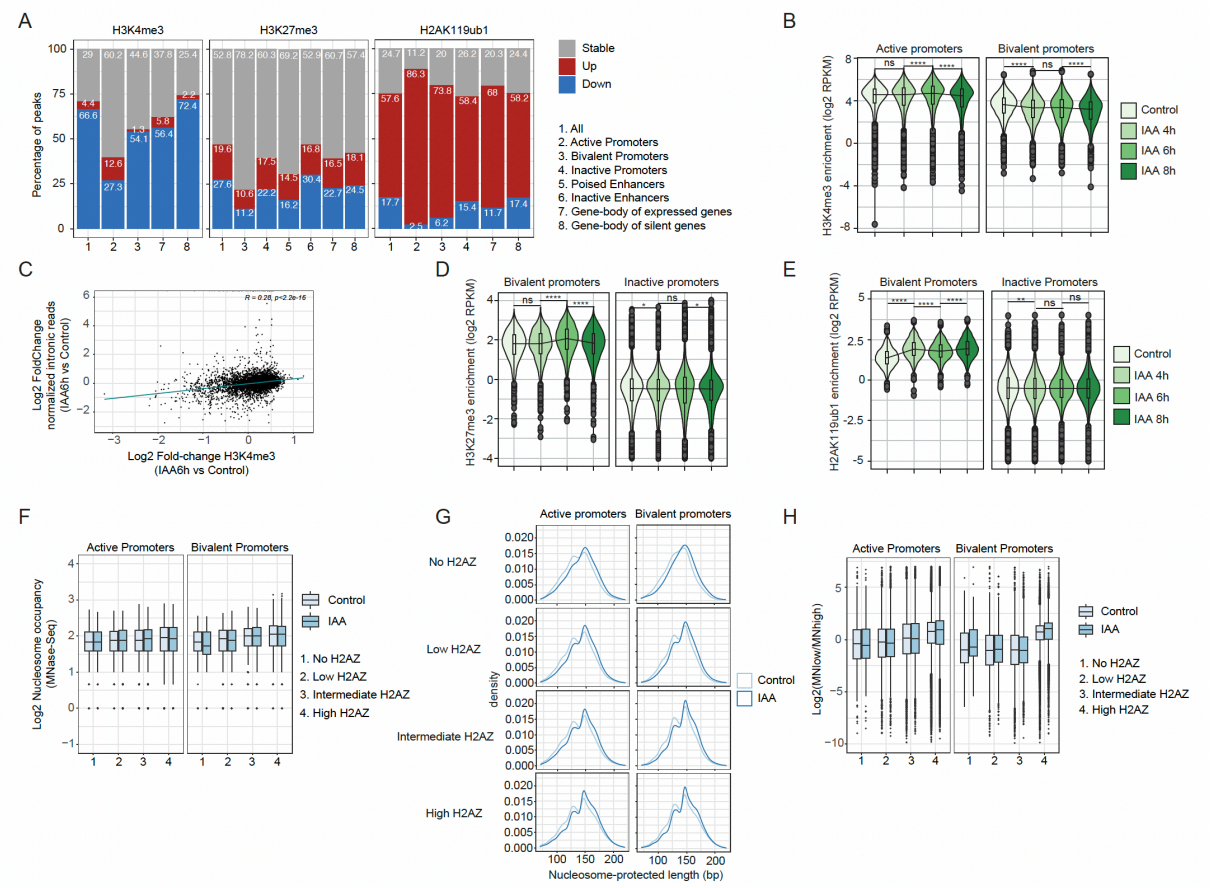

Figure 4. Impact of SRCAP/H2A.Z loss on nucleosome properties and post-translational modifications. (A) Percentage of different types of genomic regions with increased, stable or decreased H3K4me3, H3K27me3 and H2AK119ub1 marks. (B) H3K4me3 enrichment at active and bivalent promoters, in SYAT cells treated with control or IAA for 4, 6 and 8 h. (C) Scatterplot of intronic reads of genes controlled by active promoters as a function of H3K4me3 enrichment changes between 6 h of IAA treatment and control. Upper right corner: Pearson correlation coefficient. (D) and E. H3K27me3 (D) and H2AK119ub1 (E) enrichment at bivalent and inactive promoters in SYAT cells treated with control or IAA for 4, 6 and 8 h. (F) Nucleosome occupancy at promoters in SYAT cells as a function of H2A.Z levels, in control or after 4 h of IAA treatment. (G) MNase-Seq fragment densities in SYAT cells treated with control or IAA for 4 h, as a function of H2A.Z enrichment and the class of promoter where nucleosomes are localized. (H) Fragile nucleosomes in nucleosomes of different types of promoters, as

a function of H2A.Z levels. p-values were determined by a pairwise Wilcoxon test; ****: p<0.0001; ***: p<0.001; **: p<0.01; *: p<0.05, ns: non-significant.

SRCAP depletion unleashes transcription factor binding

As nucleosome properties and histone modifications affect the recruitment of transcription factors and chromatin remodelers, we next interrogated the impact of SRCAP depletion on chromatin accessibility. We performed ATAC-seq after treating SYAT cells for 2, 4, 6 or 8 h with IAA and found that overall levels of chromatin accessibility were unchanged within the first 6 h of SRCAP degradation (Figure S5A). When focusing on gene regulatory elements, we found promoters to be mostly unaffected in their accessibility, while a large number of distal intergenic regions displayed increased or decreased accessibility (Figure 5A-B). To understand the mechanisms underlying these changes, we analyzed TF footprints in accessible regions using the TOBIAS bioinformatic pipeline[56]. In wt CGR8 cells, a 4 h IAA treatment had an anecdotal impact on TF footprinting, with only 5 and 1 TF motifs footprints equally or more increased or decreased than in SYAT cells, respectively (Figure S5B, Table S3). In SYAT cells, hundreds of TF motifs already displayed significant changes in footprinting after 2 h of IAA treatment, and these alterations were very consistent across time points (Figure 5C and S5C). We found that about four times more motifs had their footprints enriched (up motifs) than depleted (down motifs) at all time points after IAA treatment (Figure 5C and S5C). Strikingly, up motifs were mostly located in distal regulatory regions, while down motifs were mostly found in promoter regions (Figure 5D and S5D). As promoter- and enhancer-regulated genes tend to be downregulated and upregulated upon SRCAP/H2A.Z depletion, respectively (Figure 3E), this suggests that changes in TF binding could drive transcriptional changes elicited by IAA treatment. We next asked whether the predominant transcriptional downregulation after mitotic IAA treatment (Figure 3G) could be caused by a shift towards more downregulated TF footprints. We thus performed 1 h of IAA or control treatment, and sorted cells enriched for the end of M-phase (Methods) and in EG1 to perform ATAC-seq prior to and concurrently to EG1 transcriptional changes, respectively. Changes in TF footprinting were more pronounced for down relative to up motifs as compared to longer IAA treatments in asynchronous cells (Figure 5E), in line with transcriptional downregulation upon mitotic SRCAP/H2A.Z loss.

As pTFs are characterized by their ability to bind nucleosomal DNA, we reasoned that their binding might be particularly sensitive to nucleosome composition. We thus quantified the number of pTFs that were enriched in the up vs downregulated motifs, using a classification of pTFs based on [57,58] (see Methods). We found that 87 out of the 376 up-TFs (23.1%) but only 7 out of the 97 (7.2%) down-TFs after 4 h of IAA treatment were known pTFs (Figure S5E). This suggests that pTF binding is generally impaired by the presence of SRCAP and/or H2A.Z.

To gain a broader view of changes in protein-DNA interactions induced by SRCAP depletion, we used an approach we (E.U. and H.L) recently developed[59] to identify proteins bound to chromatin (chromatome). We treated cells with IAA for 4 h and analyzed both changes in proteome and chromatome. In the chromatome, we found 174 proteins significantly up or downregulated. In line with TOBIAS analysis, we found more TFs to be upregulated than downregulated (Figure 5F). In the proteome analysis (Figure 3F), we did not identify any TF with significant changes in protein level correlating with changes in footprinting. This suggests that TF binding changes are not mediated by changes in their concentration. As expected, SRCAP along with other members of the SRCAP complex were depleted from chromatin (Figure 5F). However, H2A.Z levels were only slightly decreased in the whole chromatome (Figure 5F and Table S2). This suggests that H2A.Z turnover is either low and/or not SRCAP-mediated in regions that are lost in ChIP-seq experiments, such as sonication-resistant heterochromatin[60]. We then performed ChIP-seq analysis on selected TFs that significantly changed their binding in the TOBIAS analysis and/or the chromatome. ChIP-seq analysis of OCT4 and SOX2 revealed that a large fraction of their binding sites (respectively 28.2% and 42%) was more occupied upon IAA treatment, in line with TOBIAS and chromatome analysis (Figure 5G and H). However, OCT4 was reported to bind H2A.Z nucleosomes[61] and to lose binding upon H2A.Z knockdown[5]. Accordingly, sites bound by OCT4 only lost binding upon H2A.Z swapping with H2A, in contrast to sites bound by both OCT4 and SOX2 (Figure S5F). This is in line with in vitro studies showing robust OCT4 binding on canonical nucleosomes in the presence of SOX2[62,63]. Furthermore, knockdown of SOX2 using the 2TS22C cell line[64] resulted in OCT4 binding to fewer sites characterized by a higher H2A.Z enrichment (Figure S5G). This suggests that in the absence of SOX2, OCT4 favors binding to H2A.Z over H2A nucleosomes and explains the intact pioneer activity of OCT4 in the absence of SOX2 at most of its binding sites[33]. We also performed ChIP-seq on NANOG, YY1 and NFY-a and found that changes in their binding occurred as expected from TOBIAS and/or chromatome analysis (Figure 5G), with an enrichment of OCT4, SOX2 and NANOG sites displaying increased binding in distal regulatory regions (Figure S5H).

Since changes in TF binding were already maximal 2 h after induction of SRCAP degradation (Figure S5C), we reasoned that TFs could drive the gradual changes in chromatin accessibility that occurred between 2 and 4 h of IAA treatment (Figure 5A). Loss and gain of TF binding were associated with global mild decrease and marked increase in chromatin accessibility, respectively (Figure 5I), in line with the high enrichment for pTFs in the up TFs identified by TOBIAS (Figure S5E). Since OCT4 and SOX2 play a major role in regulating chromatin accessibility in mESCs[32,33], we quantified changes in chromatin accessibility at loci where their ChIP-seq signal changes upon SRCAP loss. Loci with increased OCT4 or SOX2 binding displayed more pronounced increased accessibility than loci with stable or decreased binding

(Figure S5I). We conclude that alterations in pTF binding drive changes in chromatin accessibility upon SRCAP/H2A.Z depletion.

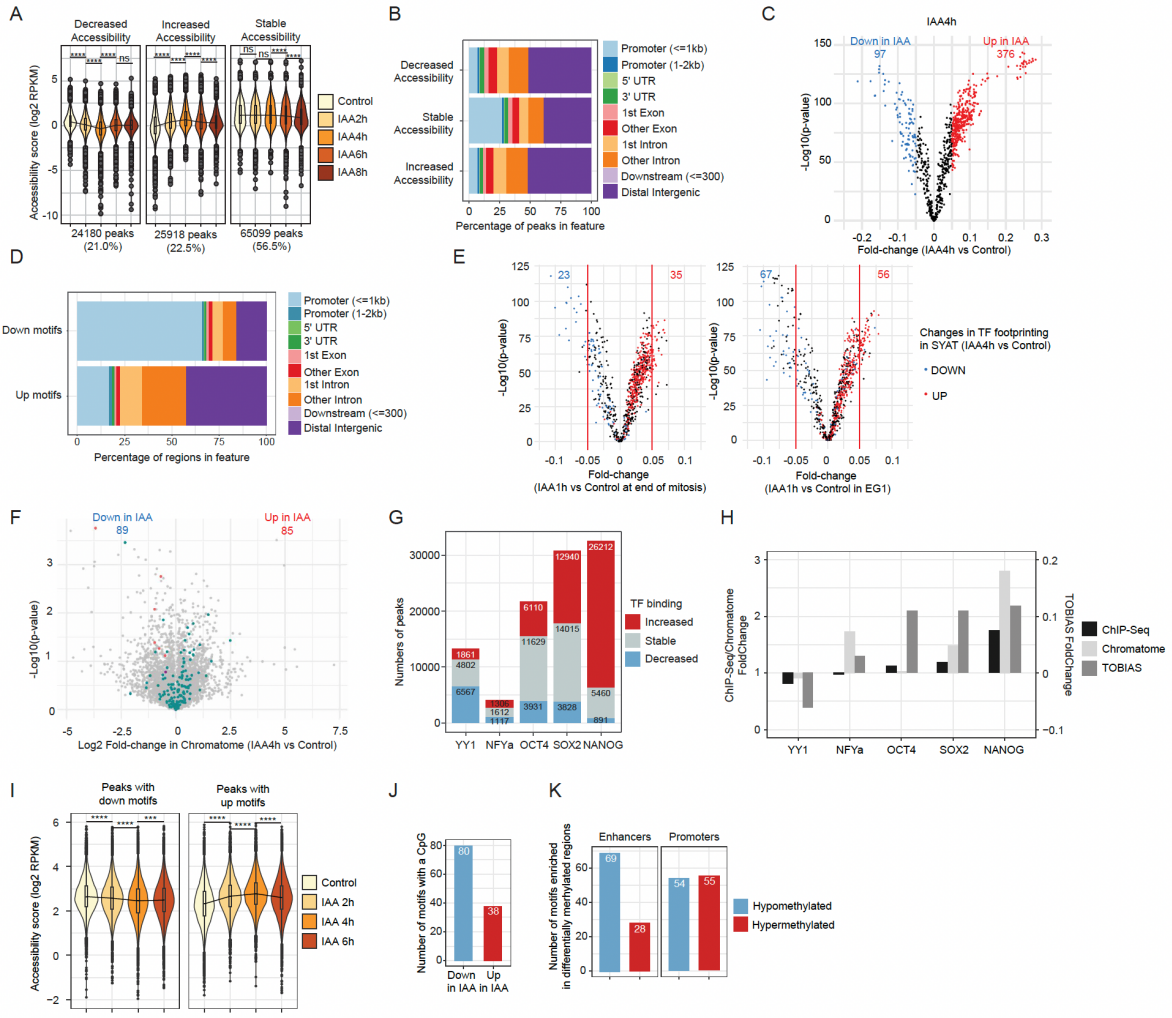

Figure 5. SRCAP depletion alters transcription factor binding. (A) Chromatin accessibility changes in SYAT cells treated with control or IAA for 2, 4, 6 and 8 h. (B) Percentage of accessible regions belonging to accessibility classes defined in A for different types of genomic regions. (C) Fold-change of TF footprinting calculated using TOBIAS in SYAT cells treated 4 h with IAA versus control. Numbers: TF motifs predicted to lose (blue) or gain (red) binding upon IAA treatment with a threshold of |FC|>0.05 and p-value < 0.0001. (D) Percentage of occurrence of all motifs, for TFs predicted to gain or lose binding in SYAT cells upon IAA treatment, for different types of genomic regions. (E) Fold-change of TF footprinting calculated using TOBIAS in SYAT cells at the end of mitosis (left panel) or EG1 (right panel). Numbers: TF motifs predicted to lose (blue) or gain (red) binding upon IAA treatment with a threshold of |FC|>0.05 and p-value < 0.0001. Colors: Predicted TF footprinting changes in SYAT treated 4 h with IAA versus control. (F) Chromatome analysis. Turquoise: TFs; red: members of SRCAP complex; purple: H2A.Z. Numbers: proteins enriched (blue) or depleted (red) from the chromatome upon IAA treatment with a threshold of |log2FC|>0.5 and p-value < 0.05. (G) Numbers of peaks with an increased or decreased TF ChIP-seq enrichment after 4 h of IAA treatment in SYAT cells. (H) Fold-change in TF binding determined by ChIP-Seq, chromatome and TOBIAS prediction analysis. (I) Chromatin accessibility changes upon IAA treatment for TF motifs predicted to gain or lose binding. (J) Number of motifs containing at least one CpG, in motifs predicted by TOBIAS to lose or gain binding upon SRCAP depletion. (K) Numbers of motifs significantly enriched in H2A.Z peaks located in promoters or enhancers and displaying cytosine hyper- or hypomethylation upon SRCAP/H2A.Z loss. p-values were determined by a pairwise Wilcoxon test; ****: p<0.0001; ***: p<0.001; ns: non-significant.

DNA methylation changes do not explain changes in TF binding upon SRCAP depletion

Since H2A.Z was proposed to antagonize DNA methylation in both plants and Metazoans[26,65], we reasoned that SRCAP loss may increase DNA methylation that could then mediate changes in TF binding. CpGs were over-represented in down motifs as compared to up motifs (Methods and Figure 5J), and strongly down TOBIAS motifs included highly methyl-sensitive TFs such as NRF1 and ZBTB33[66,67] (Table S3).

We quantified changes in DNA methylation at H2A.Z-occupied loci after 4 h of IAA treatment using Enzymatic Methyl Sequencing (EM-seq). Global DNA methylation displayed only minor changes (Figure S5J). While some promoters or enhancers displayed increased or decreased CpG methylation upon IAA treatment (Figure S5K), their accessibility was unaffected, suggesting that DNA methylation changes upon SRCAP/H2A.Z loss are not driving changes in chromatin accessibility and are unlikely to drive the observed changes in TF binding (Figure S5L). Next, we treated SYAT cells with the GSK-3484862 DNMT1 inhibitor for 5 days, which decreases DNA methylation by 80% in PSCs[68] and performed ATAC-seq on cells treated for 4 h with IAA or control. DNMT1 inhibition resulted only in a slight dampening of the impact of IAA on increased TF footprints and no impact on decreased TF footprints (Figure S5M), suggesting that changes in DNA methylation plays a minor role in regulating TF binding changes upon SRCAP/H2A.Z loss. While changes in DNA methylation do not explain changes in TF binding, we wondered if the alteration of TF binding upon SRCAP degradation could lead to changes in the level of DNA methylation. We thus identified significantly-enriched TF binding motifs in hyper- and hypomethylated H2A.Z peaks located in promoters and enhancers, and found that a large number of TF motifs were enriched in hypomethylated enhancers (Figure 5K). While we cannot exclude that H2A.Z replacement with H2A would directly impact DNA methylation on longer time scales, our results suggest that acute changes in DNA methylation upon SRCAP depletion are mainly secondary to TF activity and play only a minor role in further enhancing TF binding at hypomethylated motifs. This is also in line with a recent study showing that DNA methylation plays only a modest role in regulating enhancer activity[69].

SRCAP and H2A.Z have distinct, complementary roles in transcriptional regulation

To determine the role of SRCAP on gene regulation independently of its ability to incorporate H2A.Z into chromatin, we generated a catalytically-dead SRCAP protein (cdSRCAP) that is deficient for H2A.Z deposition by mutating 3 amino acid residues in its ATPase domain (Figure S6A). We then engineered the SYAT cell line for doxycycline (dox)-inducible expression of either wtSRCAP or cdSRCAP fused to mCherry (see Methods), hereafter referred to as wtSRCAP and cdSRCAP cell lines. We induced the expression of either wtSRCAP-mCherry

or cdSRCAP-mCherry for 24 h, and treated these cell lines with IAA or control for 4 h to deplete endogenous SRCAP. To ensure identical expression levels of wt and cdSRCAP, we then FACSorted cells with the same average mCherry fluorescence and performed ChIP-seq for H2A.Z (Figure 6A). We identified 44,769 peaks where overexpression of wtSRCAP but not cdSRCAP rescued H2A.Z levels upon IAA treatment within <10% of the control condition (see Methods) (Figure 6B). In addition, cdSRCAP cells displayed lower global H2A.Z enrichment compared to wtSRCAP cells (Figure S6B) in both control and IAA treatment conditions.

We then performed ATAC-seq after 24 h of dox and 4 h of IAA treatment in both wtSRCAP and cdSRCAP cell lines. Overall changes in chromatin accessibility upon IAA treatment were minor and comparable in both cell lines (Figure S6C). Interestingly, changes in chromatin accessibility caused by IAA treatment in SYAT cells were abolished when overexpressing wtSRCAP but also cdSRCAP (Figure S6D). This suggests that changes in chromatin accessibility upon endogenous SRCAP depletion are mostly independent of H2A.Z deposition.

To study how SRCAP and H2A.Z regulate TF binding, we then used TOBIAS to analyze TF footprints in the wtSRCAP or cdSRCAP cell lines in control or IAA conditions. K-mean clustering of TF footprinting scores yielded 6 clusters displaying different dependencies to SRCAP and/or H2A.Z levels (Figure 6C). We identified two clusters with a predominant role of SRCAP in increasing (cluster 1) or decreasing (cluster 2) TF binding (Figure 6D), as well as a role for H2A.Z in positive (cluster 3 and 4) or negative regulation (cluster 5) of TF binding at hundreds of motifs (Figure 6D). We could not find any specific enrichment of transcriptional repressors motifs in any of the clusters. Overall, SRCAP strongly prevented TF association with their motifs while H2A.Z had both enhancing and inhibitory effects on TF binding (Figure 6E). We then compared TF footprinting in rescued peaks in wtSRCAP cells treated with control or IAA, allowing us to determine the impact of different SRCAP levels on TF footprinting independently of H2A.Z levels. We found that both up and down motifs overlapped substantially with those identified upon IAA treatment of SYAT cells, confirming the prominent H2A.Z-independent role of SRCAP in regulating TF binding (Figure S6E). We also found that SRCAP and to a lesser extent H2A.Z tend to hinder TF binding at distal regulatory elements, as seen from the mostly distal localization of their TF motifs in their main inhibitory clusters 2 and 5 (Figure S6F). Conversely, both SRCAP and H2A.Z tended to stimulate TF binding at promoters, as seen from the larger fraction of TF motifs located in promoters in their main activatory clusters 1 and 4 (Figure S6F). In addition, SRCAP strongly disfavored pTF association with their motifs (112 SRCAP- vs 5 SRCAP+ motifs), while H2A.Z facilitated their binding (31 H2A.Z+ vs 15 H2A.Z- motifs) (Figure S6G). Taken together, this suggests that H2A.Z-independent activity of SRCAP plays a major role in restricting pTF binding that regulate chromatin accessibility at distal regulatory elements (Figure 5A and I).

We then compared transcriptional changes in IAA-treated cells expressing wtSRCAP or cdSRCAP. Overexpression of wtSRCAP compensated for most transcriptional changes mediated by endogenous SRCAP degradation, while cdSRCAP overexpression displayed a lesser compensatory effect (Figure S6H). We clustered genes with intronic counts significantly differing between any pair of samples, according to their changes as a function of H2A.Z and SRCAP levels in wtSRCAP or cdSRCAP cells (Figure 6F). Genes in clusters A and B were negatively regulated by H2A.Z, while genes in clusters D and E were positively regulated by SRCAP. Clusters C and F reflected conflicting effects of H2A.Z and SRCAP on gene regulation that translated into no significant differences in expression upon SRCAP degradation in SYAT cells (Figure 6G). Genes upregulated by SRCAP (clusters D and E) were associated with a general cellular function GO term (Figure S6I) and included 70 housekeeping genes. This confirmed that SRCAP plays a dominant role in activating ubiquitously expressed genes, which is in line with H2A.Z-independent upregulation of housekeeping genes reported for the Drosophila SRCAP-ortholog DOMINO during zygotic genome activation[1]. The dominant role of H2A.Z in transcriptional repression (Figure 6H) was confirmed by direct comparison of gene expression in cdSRCAP versus wtSRCAP-expressing cells in both control and IAA conditions (Figure 6I). GO enrichment analysis of genes upregulated in cdSRCAP versus wtSRCAP highlighted the specific role of H2A.Z in repressing lineage-specific genes (Figure S6J-K). We next asked whether the H2A.Z-independent SRCAP function in stimulating transcription is determinant for gene reactivation at mitotic exit, which would explain the predominant gene downregulation after SRCAP/H2A.Z depletion during mitosis (Figure 3G). We found that affected genes from all clusters stimulated by SRCAP were downregulated upon IAA treatment (Figure 6J). In contrast, 1 h-IAA treatment in late G1 cells led to transcriptional changes that were closer to those observed for longer IAA treatments in asynchronous cells (Figure S6L). This suggests that transcriptional reactivation at mitotic exit is dominated by the stimulatory effect of SRCAP, and that the inhibitory role of H2A.Z starts only later during G1 phase.

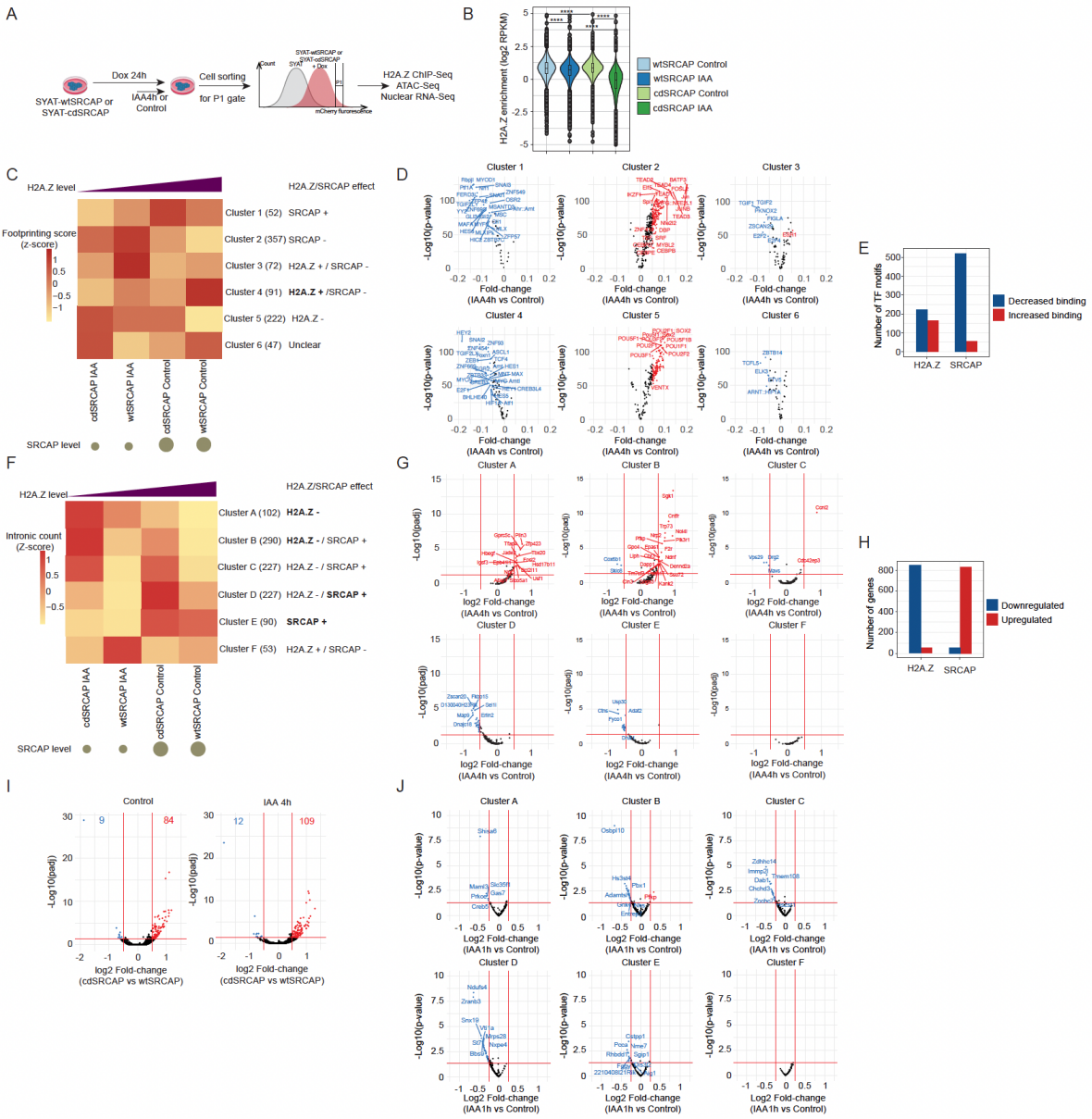

Figure 6. H2A.Z-dependent and independent functions of SRCAP. (A) Experimental procedure for dox-induced wtSRCAP and cdSRCAP expression and cell sorting. (B) H2A.Z enrichment in rescued peaks upon overexpression of wtSRCAP or cdSRCAP treated with control or IAA for 4 h. (C) Heatmap of TOBIAS footprinting scores ranked according to H2A.Z and SRCAP levels and k-mean-clustered. When SRCAP and H2A.Z display opposite effects, the dominant effect is indicated in bold. (D) Fold-change of TF footprinting calculated using TOBIAS in SYAT cells treated 4 h with IAA versus control for the six clusters determined in (C). Colored dots: TF motifs predicted to lose (blue) or gain (red) binding upon IAA treatment with a threshold of |FC|>0.05< 0.0001. (E) Numbers of TF motifs with binding increased or decreased by H2A.Z or SRCAP. (F) Heatmap of normalized intronic reads counts ranked according to H2A.Z and SRCAP levels and k-mean-clustered. When SRCAP and H2A.Z display opposite effects, the dominant effect is written in bold. (G) Fold-change of intronic reads and adjusted p-value for SYAT cells treated 4 h with IAA versus control, in the six gene clusters determined in (F). Colored dots: genes significantly downregulated (blue) or upregulated (red) with a threshold of |log2FC|>0.5 and adjusted p-value < 0.05. (H) Numbers of genes downregulated or upregulated by H2A.Z or SRCAP. (I) Fold-change of intronic reads between cdSRCAP and wtSRCAP and adjusted p-value in control (left) or IAA condition (right). Numbers: genes significantly lower (blue) or higher (red)

in cdSRCAP with a threshold of |log2FC|>0.5 and adjusted p-value < 0.05. (J) Fold-change in intronic reads in the 6 clusters defined in (F) for SYAT cells treated for 1 h with IAA or control and sorted in EG1.

Discussion

The transient nature of most DNA-protein interactions is well-established in mammalian systems[70–72]. However, the direct, acute impact of these interactions on chromatin structure and composition is much more challenging to characterize. Several studies reported that the recruitment and nucleosome-remodeling activity of the BAF complex occur continuously on a time scale of minutes[33,73,74]. Here we demonstrate dynamic SRCAP-mediated H2A.Z turnover over active and bivalent/poised regulatory elements. We found that SRCAP-dependent H2A.Z turnover rates at promoters scale with transcriptional activity of downstream genes. This is in line with transcription-mediated eviction of either full H2A.Z nucleosomes or H2A.Z-H2B dimers[36,75–77], followed by rapid re-incorporation of H2A-H2B and SRCAP-mediated loading of H2A.Z-H2B. The fact that SRCAP binds preferentially to canonical nucleosomes[23] and the correlation of its genomic occupancy with H2A.Z turnover rates (Figure 1A, H) suggest that the pace of nucleosome eviction sets the rate of SRCAP recruitment to chromatin. Surprisingly, SRCAP-mediated H2A.Z turnover is even faster during mitosis than interphase, despite very low mitotic transcriptional activity[41]. This suggests that SRCAP maintains H2A.Z levels on mitotic chromosomes by competing with transcription-independent H2A.Z eviction mechanisms that remain to be characterized.

A large arsenal of molecular machines performs a wide range of biochemical modifications of eukaryotic chromatin, which in turn can directly regulate transcription[47,48]. However, chromatin modifiers such as histone acetyltransferases and methyltransferases can also regulate gene expression independently of the modifications they catalyze[78–80], and chromatin composition also regulates the recruitment of chromatin modifiers[81–86]. Distinguishing how chromatin modifiers versus modifications contribute to gene regulation remains challenging, and this problem has so far not been addressed in the context of histone variants. Despite the initial characterization of SRCAP for its ability to recruit transcriptional coactivators[11–13], its role in gene regulation has become increasingly viewed through the lens of its H2A.Z deposition activity. This conflates the interpretation of SRCAP and H2A.Z functions in gene regulation[25,87]. The mutual regulation of their respective chromatin occupancy[23,28] and the use of slow knockdown approaches has further confounded our understanding of gene regulation by H2A.Z and SRCAP. The present study addresses these limitations and allows to clarify the specific and direct functions of SRCAP and H2A.Z in gene regulation. While both H2A.Z and SRCAP broadly regulate TF binding, we found that SRCAP plays a particularly prominent role in preventing pTF binding at enhancers while stimulating TF binding at promoters. How SRCAP regulates TF binding remains to be determined. Potential mechanisms include the recruitment of other members of the SRCAP complex known to regulate TF binding such as DMAP1, GAS41, YL-1, RUVBL1 and RUVBL2[88–91], steric hindrance to nucleosomal pTF binding[92,93] and/or nucleosome unwrapping[49,50]. We also found that, while having a positive

impact on promoter TF binding, H2A.Z plays a predominantly repressive role on transcription in line with studies suggesting that H2A.Z negatively regulates transcriptional elongation by broadening the barrier to elongating RNA Pol II[94], resulting in enhanced RNA Pol II pausing and slowing down pre-initiation complex reloading[20].

Our work reveals the coordinated activities of SRCAP and H2A.Z on TF binding and transcriptional activity as a global mechanism to repress enhancer-regulated genes and activate promoter-regulated genes. The mitotic activity of SRCAP controlling H2A.Z levels at active, bivalent and poised gene regulatory elements also suggests a role in maintaining the gene regulatory landscapes involved in self-renewal and plasticity through cell division. The dynamic interplay between SRCAP and H2A.Z thus provides an elegant strategy to maintain cell identity of PSCs by robust, yet rapidly reversible repression of lineage-specific gene expression. The requirement of SRCAP/H2A.Z for the self-renewal of multiple types of stem cells[5–7] suggests their broad involvement in the regulation of stem cell plasticity. We propose SRCAP/H2A.Z as a global gene regulatory system that acts in parallel to other epigenetic mechanisms to maintain stem cell identity and plasticity.

Acknowledgments

We thank the Gene Expression Core Facility, Flow Cytometry Core Facility, BioImaging Facility and Biomolecular Screening Facility at EPFL. We thank Dr Matthias Mann for kindly providing access to MS instrumentation, and to Dr Igor Paron and Dr Tim Heymann for their outstanding MS technical assistance. We thank Ludovica Vanzan, Nadine Vastenhouw and Nicolas Thomä for their helpful input. We are thankful for funding by the Swiss National Science Foundation grant#310030_184782 and# 310030_212197 to D.M.S. H.L and E.U are funded by the Deutsche Forschungsgemeinschaft (DFG, German Research Foundation, 213249687 - SFB1064 to H.L. (A17)). E.U. gratefully acknowledges the International Max Planck Research School for Molecular Life Sciences (IMPRS-LS) and the Research Training Group 1721 (RTG 1721) for training and support.

Authors Contributions

Conceptualization, A.T and D.M.S; Methodology, A.T, E.U and D.M.S; Formal Analysis, A.T, E.U and D.M.S; Investigation, A.T, E.U and C.D; Resources, D.M.S and H.L; Writing Original manuscript, A.T and D.M.S; Funding Acquisition, D.M.S and H.L; Supervision, D.M.S and H.L.

Methods

Key Resources Table

REAGENT or RESOURCE	SOURCE	IDENTIFIER
Antibodies		
Rabbit anti-H2A.Z	Abcam Cat#ab4174	RRID:AB_304345
Acetyl-histone H2A.Z (K4,K7,K11)	ThermoFisher Scientific Cat#PA540095	RRID:AB_2609565
Rabbit anti-H2A	Abcam Cat#ab18255	RRID:AB_470265
Rabbit anti-GFP	Abcam Cat#ab290	RRID:AB_2313768
Rabbit anti histone H3K4me3	Abcam Cat#ab8580	RRID:AB_306649
Rabbit anti histone H3K27me3	Abcam Cat#ab195477	RRID:AB_2819023
Rabbit anti histone H2AK119ub1	Cell Signaling Technology Cat#8240	RRID:AB_10891618
Rabbit anti-YY1	Cell Signaling Technology Cat#46395	RRID:AB_2799302
Mouse anti NF-Ya	Santa-Cruz Biotechnology Cat#sc-17753	RRID:AB_628018
Rabbit anti-Oct4	Cell Signaling Technology Cat#5677	N/A
Rabbit anti-Sox2	Cell Signaling Technology Cat#23064	RRID:AB_2714146
Rabbit anti-Nanog	Cell Signaling Technology Cat#8822	RRID:AB_11217637
Biological samples		
Chemicals, peptides, and recombinant proteins		
Indole-3-Acetic Acid (IAA)	Sigma-Aldrich Cat#I5148	CAS: 6505-45-9
Auxinole	MedChemExpress Cat#HY-111444	CAS:86445-22-9
GSK-3484862 (	MedChemExpress Cat#HY-135146	CAS: 2170136-65-7
Deposited data		
GSE64825	De Dieuleveult et al. 2016[95]	N/A
GSE48519	Hon et al. 2014[96]	N/A
GSE143737	Mylonas et al. 2021[20]	N/A
Experimental models: Cell lines		
CGR8 (ESC Mus musculus)	Sigma-Aldrich Cat#07032901	N/A
SYA (ESC Mus musculus)	This study	N/A
SYAT (ESC Mus musculus)	This study	N/A
ZHBTc4 (ESC Mus musculus)	Niwa et al., 2000[34]	RRID: CVCL_C715
HEK-293T	ATCC	RRID:CVCL_0063
Oligonucleotides : List provided in Table S4		
Recombinant DNA		
psPAX2	Addgene	RRID: Addgene_12260
pMD2.G	Addgene	RRID: Addgene_12259

pX330	Addgene	RRID:Addgene_42230
pMK-Ypet-AID-P2A-Hygro	This study	N/A
pLV-EF1a-OsTir1-SNAP-P2A-Puro	This study	N/A
pLV-PGK-YPet-MD	Deluz et al. 2016[97]	N/A
pLV-PGK-mCherry-MD	This study	N/A
pLV-rtTA3G-Bsd	Deluz et al. 2016[97]	N/A
pLV-TRE3G-wtSRCAP-mCherry	This study	N/A
pLV-TRE3G-cdSRCAP-mCherry	This study	N/A
Software and algorithms		
FiJi Version 2.14.0/1.54f	Schindelin et al., 2012[98]	RRID:SCR_002285
STAR Version 2.7.6a	Dobin et al., 2013[99]	RRID:SCR_015899
Picard Version 2.23.7	Broad Institute	RRID:SCR_006525
MACS Version 3.0.0a7	Zhang et al., 2008[100]	RRID:SCR_013291
DeepTools Version 3.5.1	Ramírez et al., 2016[101]	RRID:SCR_016366
Bedops Version 2.4.41	Neph et al., 2012[102]	RRID:SCR_012865
BEDtools Version 2.30.0	Quinlan and Hall, 2010[103]	RRID:SCR_006646
SAMtools Version 1.14	Li et al., 2009[104]	RRID:SCR_002105
DANPOS2 Version 3.1.1	Chen et al. 2013[105]	RRID:SCR_015527
Bwa-Meth	Pedersen et al. 2014[106]	RRID:SCR_010910
MethylDackel Version 0.5.3	https://github.com/dpryan79/MethylDackel	
MethylKit Version 1.28.0	Akalin et al. 2012[107]	RRID:SCR_005177
DeSeq2 Version 1.42.1	Love M.I et al. 2014[108]	RRID:SCR_015687
edgeR Version 4.0.11	Robinson et al., 2010[109]	RRID:SCR_012802
limma Version 3.58.1	Ritchie et al., 2015[110]	RRID:SCR_010943
R studio Version 2023.12.0+369		RRID:SCR_000432
Cluster Profiler Version 4.10.1	Yu et al. 2012[111]	RRID:SCR_016884
ggplot2 Version 3.5.0	Wickham, 2009[112]	RRID:SCR_014601
ggrepel Version 0.9.5	Slowikowski K, 2024	
biomaRt Version 2.58.2	Durinck et al., 2005[113]	RRID:SCR_002987
TOBIAS Version 0.13.3	Bentsen et al.,2020[56]	
SEA Version 5.5.5	Bailey and Grant, 2021[114]	RRID:SCR_001783

Cell culture

CGR8 mouse ES cells (Sigma, Cat#07032901-1VL) and ZHBTc4 mouse ES cells [34] were routinely cultured at 37 °C and 5% CO_2 on cell culture-treated dishes coated with 0.1% gelatin (Sigma #G9391-100G) using the following culture medium: GMEM (Sigma #G5154-500ML) supplemented with 10% ES-cell qualified fetal bovine serum (Gibco #16141–079), 1% nonessential amino acids (Gibco #11140–050), 2 mM L-glutamine (Gibco #25030–024), 2 mM sodium pyruvate (Sigma #S8636-100ML), 100 µM 2-mercaptoethanol (Sigma #63689–25 ML-F), 1% penicillin and streptomycin (BioConcept #4–01 F00-H), in-house produced leukemia inhibitory factor (LIF), CHIR99021 (Merck #361559–5 MG) at 3 µM and PD184352 (Sigma #PZ0181-25MG) at 0.8 µM. Cells were passaged by trypsinization (Sigma #T4049-100ML)

every two to three days. Before all experiments, mESC medium was changed to Serum LIF medium: GMEM (Sigma #G5154-500ML) supplemented with 10% ES-cell qualified fetal bovine serum (Gibco #16141–079), nonessential amino acids (Gibco #11140–050), 2 mM L-glutamine (Gibco #25030–024), sodium pyruvate (Sigma #S8636-100ML), 100 µM 2-mercaptoethanol (Sigma #63689–25 ML-F), penicillin and streptomycin (BioConcept #4–01 F00-H), in-house produced leukemia inhibitory factor (LIF). SYAT cells were cultured routinely with 200nM Auxinole (MedChemExpress #HY-111444) (Control condition) to avoid basal degradation of SRCAP. For SRCAP degradation, SYAT cells were treated for 1, 2, 4, 6 or 8 h with 500 µM Indole-3-Acetic Acid (IAA, Sigma-Aldrich #I5148). For induction of Oct4 knockdown in ZHBTc4 cells, 1 µg/mL Doxycycline was added for 9 or 12 h prior cell collection. For DNMT1 inhibition, SYAT cells were treated with 2 µM GSK-3484862 (MedChemExpress #HY-135146) for 5 days before performing ATAC-seq. All used cell lines were tested every 6 months for the absence of Mycoplasma by Eurofins Genomics.
For imaging, cells were plated on Laminin (1/10 dilution of Biolaminin (BioLamina, LN511-0202) in PBS). Prior imaging, medium was replaced by FluoroBrite DMEM (ThermoFisher, #A18967–01) supplemented with 10% ES cell-qualified fetal bovine serum (ThermoFisher, #16141079), 2 mM sodium pyruvate (Sigma-Aldrich, #113–24–6), 1% non-essential amino acids (ThermoFisher, #11140035), 1% penicillin/streptomycin (BioConcept, #4–01F00H), 2 mM L-glutamine (ThermoFisher, #25030–024), 100 µM 2-mercaptoethanol (Sigma-Aldrich, #63689–25ML-F) and LIF.

Lentiviral vector production

Lentiviral vectors were produced by transfection of HEK 293T cells with the envelope (psPAX2, Addgene #12260), packaging (pMD2.G, Addgene #12259)[115], and lentiviral construct of interest using Calcium Phosphate transfection, as described previously[116]. Viral vectors were concentrated 120-fold by ultracentrifugation at 20’000 x *g* for 120 min at 4°C. 50’000 cells in 500 µL of medium in a 24-well plate were transduced with 50 µl of concentrated lentiviral vector particles to generate stable cell lines.

Generation of SYA and SYAT cell lines

The SYA cell line was generated using CRISPR/Cas9-mediated homology-directed repair (HDR). A SRCAP gRNA designed using CRISPOR[117] to target the C-terminal part of mouse SRCAP was added in pX330-gRNA vector (pX330-gRNA was a gift from Charles P. Lai (Addgene plasmid #158973)) by digestion with BbsI to build pX330_SRCAP. The Ypet_AID_P2A_Hygromycin-resistance cassette was amplified with primers containing 60bp homology arms corresponding to the carboxy-terminal part of SRCAP and 2µg of amplicons were co-transfected in $1.5x10^6$ CGR8 ESC together with 2 µg of pX330-SRCAP using

Lipofectamine 3000 (ThermoFisher Scientific #L3000008). Cells were selected by addition of 150 µg/mL Hygromycin 72 h post-transfection for a week before individual clones were picked. gDNA was extracted using Direct PCR Lysis (Viagen Biotech, #301-C) and incubated 2 h at 55°C, 30 min at 85°C followed by 5 min at 95°C. Clones were characterized by PCR using primers annealing to the SRCAP locus and in the knock-in cassette (Table S4), followed by visualization of the Ypet signal intensity and nuclear localization by live imaging using the YFP channel on a IN Cell Analyzer 2200 apparatus (GE healthcare). One homozygous clone of SYA cells was then transduced with a lentiviral vector containing EF1a-OsTir1_SNAP-P2A-puro and selected with 2 µg/ml of Puromycin (Gibco A11138-03) for a week. To select for cells efficiently degrading SRCAP upon IAA treatment, SYAT cells were treated for 2 h with IAA prior sorting for Ypet negative cells.

SRCAP constructs and cell line generation

SRCAP was amplified from cDNA of CGR8 cells in 3 separate PCR fragments. For the catalytically-dead mutant, the mutations were introduced in the Rev primer of the first fragment and the Fw primer of the second fragment (See Table S4 for primer sequences). The three fragments and the pLV-TRE3G-mCherry cut with SalI upstream of the mCherry coding sequence were assembled using In-fusion cloning (Takara Bio # 638947) and the obtained products were transformed into home-made HB-101 competent bacteria. Clones were then screened by PCR for the presence of full length SRCAP and sequenced to verify the presence of the mutated sequence. Correct clones were used to produce lentiviral particles, which were used to transduce SYAT cells together with a lentiviral vector expressing rtTA3G and a blasticidin resistance. To select for clones expressing the construct, after selection with 5µg/mL Blasticidin for a week, cells were treated with 1µg/mL of dox for 24 h to induce expression of SRCAP-mCherry, prior to cell sorting for mCherry-positive cells and isolation of single cells. One clone for wtSRCAP and one clone for cdSRCAP were selected by FACS for similar mCherry levels. Prior to all experiments, wtSRCAP and cdSRCAP were induced with 1 µg/mL Doxycyline for 24 h, treated with 500 µM IAA for 4 h or left in 200 µM Auxinole (Control) and sorted for similar and high mCherry expression just before performing ChIP-Seq, ATAC-Seq or nuclear RNA-Seq.

FACS for different cell cycle phases

For mitotic ChIP, $12x10^6$ million cells were collected by mitotic shake-off, fixed 10 min with 1% formaldehyde (ThermoFisher #28908) at room temperature (RT) prior to quenching with 250 mM Tris-HCl pH8. Next, staining with 50 mM Hoechst33342 (Thermo Fisher Scientific #H3570) was performed for 15 min at RT. Cells were then permeabilized by addition of ice-cold 70% ethanol and stained with an anti-H3S10ph antibody (Merck-Millipore, 05-1336) diluted 1:1000

for 1 h at 4°C. Samples were stained with Alexa-Fluor 647 anti-rabbit (H+L) secondary antibody (ThermoFisher Scientific #A-31571) for 45 min at 4°C. Mitotic cells were selected by FACS as Hoechst-high and H3S10ph-positive. For other phases of the cell cycle, we used CGR8 cells stably expressing Ypet-MD or SYAT cells stably expressing mCherry-MD stained with Hoechst as previously described, followed by sorting according to Hoechst and Ypet/mCherry intensities: Hoechst low-Ypet/mCherry low cells being in early G1 phase, Hoechst low-Ypet/mCherry high in late G1 phase, intermediate Hoechst in S phase and high Hoechst in G2M phase. For sorting of cells at the end of mitosis, SYAT cells expressing mCherry-MD and stained with Hoechst were selected for Hoechst high-mCherry low intensities. All FACS were performed on a FACSAria II or a FACSAria Fusion (BD Biosciences).

Immunofluorescence

SYAT or wt CGR8 cells were plated on 1:10 diluted Biolaminin (BioLamina, LN511-0202) in DPBS (Gibco, 14040091) in 96-well plates with black walls or 3.5 mm dishes. Cells were fixed with 2% Formaldehyde diluted in DPBS for 30 min at RT. Permeabilization was then performed by addition of a solution of 0.5% Triton X-100 (AppliChem, A1388,0500) for 30 min before addition of blocking solution (BSA 1% (Sigma-Aldrich, A7906) in DPBS) for 30 min. An anti-H2A.Z antibody (Abcam ab4174) was diluted 1:1000 in blocking solution prior to incubation overnight at 4°C, followed by three washes with 0.1% Tween-20 diluted in DPBS. The secondary antibody Alexa-Fluor-647 Chicken anti-rabbit IgG (H+L) (ThermoFisher Scientific #A-21443)**,** was diluted 1:1000 in blocking buffer and incubated for 1 h at RT. Cells were then washed three times with 0.1% Tween-20 diluted in DPBS and twice with DPBS before addition of DAPI-Fluoromount G (SouthernBiotech, #0100-20). Imaging was performed on an IN Cell Analyzer 2200 apparatus (GE healthcare) a 20X magnification objective, using the YFP fluorescence channel for YPet detection, the Cy5 fluorescence channel for AF-647 detection and DAPI fluorescence channel for DAPI detection. For high magnification imaging of mitotic chromosomes, imaging was performed at the Bio-Imaging facility at EPFL on a spinning disk microscope (Visitron CSU-W1) with a 60X objective. For image quantification, the Fiji software[98] was used to subtract background and manually determine the area of the region of interest (ROI) and the intensities for the different channels. For each channel, integrated intensities were calculated by multiplying the mean fluorescence intensity by the area of the ROI. Around 50 cells were quantified for each treatment condition and phase.

Pluripotency assay and RT-qPCR

600 SYAT or CGR8 cells were plated in 6-well plates and cultured in GMEM-Serum-2I-LIF for 5 days. Cells were stained with Phosphatase Alkaline staining kit (Merck-Millipore, SCR004) according to the manufacturer instructions.

For RT-qPCR experiments, RNA was extracted from $3x10^6$ SYAT or CGR8 cells with the Rneasy Plus Mini Kit (Qiagen, #74134). Reverse transcription was performed on 1 µg RNA using oligodT (Thermo Fisher Scientific #SO131) and Maxima H minus First Strand cDNA synthesis (Thermo Fisher Scientific #K1652). RT was diluted 1/10 prior to qPCR. Primers used to amplify *Rps5*, *Zfp42*, *Pou5f1*, *Sox2*, *Nanog*, *Esrrb* and *c-Myc* are detailed in Table S4. Plates were assembled using an automated Hamilton liquid handling platform and analyzed on a QuantStudio 7 (Applied Biosystem). Relative quantifications were obtained by normalization on *Rps5* mRNA levels.

ChIP-Seq

For histones and histone post-translational modifications, cells were fixed for 10 min with 1% formaldehyde at RT. For transcription factors, cells were fixed with 2 mM disuccinimidyl glutarate (Thermo Fisher Scientific #20593) for 50 min and in 1% formaldehyde for 10 min. In both cases, fixation was quenched with 250 mM Tris-HCl pH8. All fixed cell pellets except mitotic samples were kept on ice and resuspended in Lysis Buffer 1 (50 mM HEPES-KOH pH 7.4, 140 mM NaCl, 1 mM EDTA, 0.5 mM EGTA, 10% Glycerol, 0.5% NP-40, 0.25% Triton X-100 supplemented with Protease inhibitor cocktail (Sigma #P8340-1ML) at 1:100 dilution), incubated 10 min at 4°C, spun down at 1700 x *g*, and resuspended in LB1 a second time, spun down and resuspended in Lysis Buffer 2 (10 mM Tris-HCl pH 8.0, 200 mM NaCl, 1 mM EDTA, 0.5 mM EGTA supplemented with Protease inhibitor cocktail (Sigma #P8340-1ML) at 1:100 dilution), incubated for 10 min at 4°C, spun down and washed without disturbing the pellet twice with SDS shearing buffer (10 mM Tris-HCl pH 8.0, 1 mM EDTA, 0.15% SDS supplemented with Protease inhibitor cocktail (Sigma #P8340-1ML) at 1:100 dilution)) and finally resuspended in SDS shearing buffer. For mitotic samples, cell pellets were washed twice in SDS shearing buffer and then resuspended in SDS Shearing buffer. Chromatin was sonicated for 20 min at 5% duty cycle, 140 W, 200 cycles or for sorted samples 10 min 10% duty, 75W, 200 cycles on a Covaris E220 focused ultrasonicator. ChIPs were then performed using ChIP-IT High Sensitivity kit (Active motif, #53040) by following manufacturer instructions. 10 ng of Drosophila spike-in chromatin (Active motif, 53083) and 0.5µg of spike-in antibody (anti-H2Av, Active motif, 61686) were processed together with mESC chromatin (1.5 µg for ChIP-seq on mitotic cells and matching asynchronous cells, 4 µg for the other H2A.Z and H2A ChIP-seq, 2 µg for H3K4me3, H3K27me3 and H2AK119ub1 and 5 µg for ChIP-seq against TFs) as an internal experiment calibrator[118]. Libraries were prepared with the NEBNext Ultra II DNA Library Prep Kit (NEB #E7645) and sequenced on an Illumina NextSeq 500 using 75-nucleotide read length paired-end sequencing.

CUT&Tag

CUT&Tag experiments were performed in duplicates using the CUT&Tag-IT Assay Kit (Active Motif #53160) and following manufacturer instructions. Briefly, 200,000 SYAT cells were bound on Concanavalin A beads prior to incubation overnight with 1:50 anti-GFP rabbit antibody (Abcam #ab290). Next, cells were incubated with a secondary antibody, pA-Tn5-transposomes, and washed according to manufacturer instructions. Transposition was subsequently performed for 1 h at 37°C, and transposed DNA was purified prior to Library Preparation and size exclusion with SPRI beads using a 0.5X ratio while keeping the unbound fraction and 1X ratio on the left side, taking the bound fraction. Libraries were sequenced on an Illumina NextSeq 500 using 75 nucleotide read-length paired-end sequencing.

ATAC-Seq

All ATAC-seq experiments were performed in biological duplicates. 50,000 cells were collected either directly after trypsinization or after sorting as described above, and subjected to ATAC-seq as described previously[119]. All centrifugation steps were done at 800 x *g* at 4°C. Briefly, cells were centrifuged for 5 min and washed with cold PBS, then centrifuged for 5 min and resuspended in cold lysis buffer (10 mM Tris-HCl pH 7.4, 10 mM NaCl, 3 mM MgCl2, 0.1% NP-40), and centrifuged for 10 min. Subsequently, nuclei were resuspended in a solution of 0.5 mM Tn5 (in-house preparation according to [120]) in TAPS-DMF buffer (10 mM TAPS-NaOH, 5 mM Mgcl2, 10% DMF) and incubated for 30 min at 37°C. DNA was immediately purified using column purification (Zymo #D4004) and eluted in 10 ml nuclease-free water. Transposed DNA was amplified in a solution containing 1X NEBNextHigh Fidelity PCR Master Mix (NEB #M0541L), 0.5 µM of Ad1.1 universal primer, 0.5 µM of Ad2.x indexing primer and 0.6x SYBR Green I (Thermo Fisher Scientific #S7585) using 72°C for 5 min, 98°C for 30 s, and 5 cycles of 98°C for 1 s, 63°C for 30 s, and 72°C for 60 s. 10 µl of amplified DNA was analyzed by qPCR to determine the total number of cycles to avoid amplification saturation and accordingly amplified with additional 3–7 cycles at 98°C for 10 s, 63°C for 30 s, and 72°C for 60 s. DNA was purified using column purification (Zymo #D4004) and size-selected by taking the unbound fraction of 0.55X AMPure XP beads (Beckman Coulter #A63880) followed by the bound fraction of 1.2X AMPure XP beads. Libraries were sequenced on an Illumina NextSeq 500 using 75 nucleotide read-length paired-end sequencing.

Nuclear RNA-Seq

All RNA-Seq experiments were performed in biological duplicates. Following cell collection and wash in PBS, cell pellets were resuspended in 500 µL Nuclear RNA lysis buffer (10 mM Tris pH 7.4, 10 mM NaCl, 3 mM MgCl2, 1% BSA (Merck, #B9000S), 0.1% Tween (Fisher Scientific, #10113103), 1 mM DTT (Merck, #646563), 0.5 U/µl Protector RNase Inhibitor (Merck, #3335399001), 0.1% NP-40, 0.01% Digitonin (Invitrogen, #BN2006)) and incubated 5 min on

ice. Then 500 µL Nuclear RNA wash buffer (10 mM Tris pH 7.4, 10 mM NaCl, 3 mM MgCl2, 1% BSA (Merck, #B9000S), 0.1% Tween (Fisher Scientific, #10113103), 1 mM DTT (Merck, #646563), 0.5 U/µl Protector RNase Inhibitor (Merck, #3335402001) were added before spinning down cells at 300 x *g* 4°C for 5 min. Two more washes with Nuclear RNA wash buffer were performed before proceeding to RNA extraction using the Rneasy Plus Micro Kit (Qiagen, #74034) with the addition of an on-column DNAse digestion (Qiagen, #79254). Sequencing libraries were prepared by the EPFL Gene Expression Core Facility using the NEBNext Ultra II Directional RNA Library Prep Kit for Illumina (NEB, #E7760S), and sequenced on a NovaSeq6000 using 75-nucleotide read length paired-end sequencing.

MNAse-Seq

All MNAse-Seq experiments were performed in triplicates according to the following protocol[121]. Briefly, Micrococcal Nuclease S7 (Roche #10107921001) was resuspended to 15 U/µL in 20 mM Tris-HCl pH 7.5, 50 mM NaCl, 50% Glycerol. For high digestion condition, MNase was diluted at 100 U/mL in MNase Digestion buffer (50 mM Tris-HCl pH 8, 150 mM sucrose, 50 mM NaCl, 5 mM $CaCl_2$). For low digestion condition, MNase was diluted at 6.25 U/mL in MNase Digestion Buffer. SYAT cells were treated for 4 h with 500 µM IAA or 200 nM Auxinole before collection. $5x10^6$ cells were used for each MNase digestion condition. After cell collection, cell pellets were resuspended in 50 µL Resuspension Buffer (35 mM HEPES pH 7.4, 150 mM sucrose, 80 mM KCl, 5 mM KH_2PO_4, 5 mM $MgCl_2$, 0.2% NP-40). Then, 500 µL of MNase solution were added to the cells and incubated for exactly 10 min at 37°C before inactivation of MNase by addition of 11 µL of 0.5 M EDTA to the reaction. Next, 550 µL of Lysis Buffer (50 mM Tris-HCl pH 8, 1% SDS, 10 mM EDTA) was added and samples were incubated on ice for 10 min. After addition of 1.1 mL DNAse-free water, samples were digested for 2 h at 37°C with RNase (50 µg per reaction). Finally, 3200 U of Proteinase K were added, and digestion was performed at 56°C for 2 h. Digested DNA was purified using DNA Purification kit (Active Motif #58002). Then, 500 ng of DNA for the High digestion condition and 1500 ng of DNA for the Low digestion condition were loaded on a 1.5% agarose gel and the band below 200bp was cut out and gel-purified. Library preparation was carried out on the purified DNA using NEBNext Ultra II DNA Library Prep Kit (NEB #E7645) and sequenced at 100 million reads per sample on a NovaSeq6000 using 75-nucleotide read length paired-end sequencing.

Enzymatic Methyl-Sequencing

EM-Seq experiments were performed in duplicate. Genomic DNA was extracted using a DNeasy Blood and Tissue kit (Qiagen #69504) and repurified using a DNA Clean and Concentrator-5 Kit (Zymo #D4004). Next, 200 ng of purified genomic DNA were sonicated for 90 s, 10% duty, 140 W, 200 cycles on a Covaris E220 focused ultrasonicator and were

subsequently processed using NEBNext Enzymatic Methyl-Seq kit (NEB #7120) following the manufacturer protocol. Libraries were sequenced at 200 million reads per sample on a NovaSeq6000 using 75-nucleotide read length paired-end sequencing.

Whole Proteome and chromatome analysis by Mass Spectrometry

The whole proteome and chromatome sample preparation, liquid chromatography followed by tandem mass spectrometry (LC-MS/MS) and data analysis were performed as previously described in [59], with a few adjustments:

For the whole proteome-chromatome-matched sample collection, 7 x 10^6 embryonic stem cells were harvested per condition and replicate. The cells were washed with PBS and split into two parts: 2 x 10^6 cells for whole proteome analysis and 5 x 10^6 cells for chromatome analysis.

Liquid chromatography was performed using the EvosepONE system with a 15 cm × 150 µm column containing 1.9 µm C18 beads (PepSep). Each sample (200 ng) was loaded onto Evotips according to the manufacturer's protocol. The gradient length was 44 minutes (30SPD). The column temperature was maintained at 40°C, and electrospray ionization was achieved using a stainless-steel emitter (30 µm inner diameter) at 2.2 kV.

Mass spectrometry was conducted on an Orbitrap Exploris™ 480 mass spectrometer (Thermo Fisher Scientific) in data-independent acquisition (DIA) mode. MS1 acquisitions were performed as previously described, using an orbitrap resolution of 120,000 with a scan range of 350-1400 m/z and a maximum injection time of 45 ms. For the MS2 acquisition, adjustments were made to accommodate the shorter LC gradient. Specifically, 49 scan events were performed with isolation windows of 13.7 m/z at an orbitrap resolution of 15,000. The normalized AGC target was set to 3000%, and the maximum injection time was 22 ms. The precursor mass range was maintained at 361-1033 m/z.

The list of TF was determined using a list of proteins associated with the GO terms DNA-binding transcription factor activity (GO:0003700) and Sequence-specific DNA binding (GO:0043565).

ChIP-Seq and CUT&Tag analysis

Newly-generated ChIP-sequencing libraries, as well as ChIP-Seq for BRG1, Ep400, CHD4, H3K27ac, H3K4me1, H2A.Z.1 and H2A.Z.2 that were reanalyzed, were mapped to mm10 version of Mus musculus genome or version BDGP6 of Drosophila Melanogaster genome, using STAR[99] with parameters --alignMatesGapMax 2000 --alignIntronMax 1 --alignEndsType EndtoEnd --outFilterMultimapNmax 1. Duplicated reads and reads not mapping to chromosome 1-19 and X or Y were removed using Picard (Broad Institute). For the generated

Drosophila alignments bam file, the number of reads was determined, and normalization factors were calculated to bring all the Drosophila bam files to the same number of reads. These normalization factors were then applied to downsample alignment files mapped on the mouse genome using SAMTools[104]. Peak calling was then performed on these downsampled bam files using MACS2[100] with settings -f BAMPE -g mm, regions contained in mm10 blacklist from ENCODE consortium were excluded. Scores were determined from downsampled bam files using the bamCoverage function from DeepTools[101] with setting --normalizeUsing RPKM. For score comparison, a bed file regrouping all peaks called in at least one condition was generated, and enrichment was calculated in these defined regions using the multiBigwigSummary function from DeepTools. For classification based on differences of peak amplitude between two time points of IAA treatment or with control, peaks were considered to be different in amplitude if there was a variation of at least 20% of enrichment score in peaks (RPKM-normalized) for H2A.Z, H3K4me3, H3K27me3 and H2AK119ub or at least 30% for YY1, NFYa, OCT4, SOX2, NANOG and H2A.Z in mitotic and asynchronous cells treated with IAA for 1 h or control.

For H2A.Z ChIP-Seq performed across the cell cycle, promoter and enhancer clusters were determined by k-mean clustering of the log2 fold-change of the signal between G2 and M phase together with log2 fold-change of the signal between M and EG1 phases, using the plotHeatmap function of DeepTools.

For H2A.Z ChIP in wtSRCAP or cdSRCAP-expressing SYAT cells, peaks were considered as rescued if the difference between IAA and Control enrichment scores was higher (with a 10% margin) in cdSRCAP compared to wtSRCAP.

In boxplots, the edges of the box represent respectively the first and third quartiles (Q1 and Q3), the bar represent the median value and the dots are the outlier values (lower than Q1-1.5xInterquartile-range, higher than Q3+1.5xInterquartile-range).

Establishment of reference bed files

The list of promoters was determined from a list of TSS in mm10 genomes (obtained from refTSS from the UCSC Genome Browser) that was enlarged from 1kb upstream the TSS and 500pb downstream. To determine the list of active promoters, this list was crossed with H3K4me3 peaks without any repressive histone marks, for bivalent promoters with peaks from H3K4me3 and H3K27me3 ChIP-Seq and for inactive promoters with H3K27me3 peaks that overlapped with no activating histone marks. To determine active enhancers, promoter regions were excluded and then H3K27ac peaks were crossed with H3K4me1 peaks. Poised enhancers were determined by crossing H3K4me1 enrichment with H3K27me3 enrichment. Regions outside promoters and without H3K4me1 enrichment were classified as inactive enhancers. For analysis using all enhancers grouped together, the list from the FANTOM5

consortium was used, or alternatively we used the list from Enhancer Atlas[122] established in J1 mESCs when promoter-enhancer loop information was required. To determine the number of promoter-enhancer loops, the number of enhancers interacting with one given gene was computed using the Enhancer Atlas list, separating upregulated genes from downregulated genes upon SRCAP depletion.

The list of TSS was enlarged from 20bp upstream and 20bp downstream of the TSS to determine the position of the TSS-nucleosome. Then the 400pb upstream of this position and 400pb downstream were considered as regions of positioning for the -1 or +1 nucleosomes, respectively.

Enhancer RNAs were defined as follows: the middle position of enhancers from the J1 enhancer list was determined and RNA reads falling into 3kb upstream and downstream were extracted, except those falling into exons and long non coding RNA (list taken from LncRBase, http://bicresources.jcbose.ac.in/zhumur/lncrbase/).

H2A.Z.1-only, H2A.Z.2-only and shared peaks were determined by intersecting bed files generated from ChIP-Seq reanalysis of data from [20] using the bedtools intersect function. OCT4-dependent, SOX2-dependent, and co-dependent regions were extracted from a previous study[33].

MNAse-Seq analysis

MNAse-Seq libraries were mapped and filtered as described for ChIP-Seq. Nucleosome positions were determined using the dpos function from DANPOS2[105]. Enrichment scores were computed using the bamCoverage function from DeepTools[101] with the setting --normalizeUsing RPKM. For all nucleosomes determined using DANPOS, the H2A.Z enrichment score was calculated, and nucleosomes were classified into “No H2A.Z” (3% lowest H2A.Z scores), “low H2A.Z” (1st quartile except “No H2A.Z”), “High H2A.Z” (Upper quartile) and “Intermediate H2A.Z” (remaining nucleosomes). These nucleosomes were further classified depending on whether they were in promoters or enhancers and according to the activity of these regulatory regions. Occupancy data were extracted from comparison of MNhigh and MNlow datasets using DANPOS. For MNase sensitivity, MNhigh and MNlow scores were determined for all nucleosomes using the multiBigwigSummary function from DeepTools and the MNlow over MNhigh ratio was calculated. For fragment length analysis, subsets of bam files were generated according to H2A.Z enrichment and regulatory regions using the samtools view function with parameters -b -h -L. The lengths of the fragments in the bam files were then determined with the samtools view -f66 | cut -f 9 command line.

Nuclear RNA-Seq analysis

Nuclear RNA-Seq libraries were mapped to the mm10 mouse genome using STAR. Exon coordinates were gathered from GENCODE annotation from vM25 of the UCSC Genome Browser. Introns coordinates were determined by subtracting exon coordinates from full length gene bodies using a script generated in a previous study (https://github.com/charitylaw/Intron-reads, [123]). Gene counts were then determined using the featureCounts function [124] from the R package Rsubread. Differential enrichment analysis as well as normalization of results using the lfcShrink function with type ="normal" were performed using DeSeq2[108]. Reads counts were normalized on introns length and in transcript per million (TPM) for analysis of absolute RNA levels in control condition.

The bivalent genes list was determined from the list of bivalent promoters. The list of housekeeping genes was taken from a previous study[125]. Finally, the list of genes associated with pluripotency, mesoderm commitment, ectoderm commitment and endoderm commitment were compiled from Datanode using the terms "Mechanism associated with pluripotency (WP1763)", "Mesodermal commitment pathway (WP2857)", "Ectoderm differentiation (WP2858)" and "Endoderm differentiation (WP2853)", respectively.

For k-mean clustering of gene expression between wtSRCAP and cdSRCAP treated with IAA or control, intronic reads count for genes affected in at least one condition were normalized by DeSeq2 using the median of ratios method. Then for each gene, the z-scores across samples were computed. Kmean clustering was next performed using the pheatmap function from pheatmap R package (https://CRAN.R-project.org/package=pheatmap) using a fixed number of 6 clusters.

EM-Seq analysis

Libraries were mapped using bwa-meth from Bwa (from Brent Pedersen, https://github.com/brentp/bwa-meth). CpG methylation was then calculated using MethylDackel (https://github.com/dpryan79/MethylDackel) before analysis of Differential methylation using MethylKit[107]. CpG methylation was computed for H2A.Z peaks located in promoters and enhancers and if the percentage of methylation was increased or decreased by 5%, regions were considered as hypermethylated or hypomethylated, respectively.

ATAC-Seq analysis

ATAC-Seq libraries were mapped and filtered as described for ChIP-Seq. The alignment files were subsequently downsampled so that all files contain the same total number of reads. Accessible peaks were then called, and scores were computed as described above for ChIP-Seq. Differentially-accessible regions were determined among peaks that had been called in at least one condition, for scores that varied from at least 30% between control and 4 h of IAA treatment.

TOBIAS analysis

For TOBIAS analysis, alignment files from ATAC-Seq were normalized with trimmed mean of M values (TMM) using calcNormfactors from edgeR with the TMM method followed by downsampling using SAMTools. Then, a correction of Tn5 bias was performed using TOBIAS ATACCorrect in all accessible regions in SYAT treated with control or IAA, excluding mm10 ENCODE-blacklisted regions. Footprints were then assessed with TOBIAS FootprintScore in the same regions. Finally, conditions were compared using TOBIAS BINDetect on the same regions or H2A.Z-rescued regions when specified, using the Jaspar2022[126] non-redundant core list of motifs to which the Nanog motif (UN0383.1) was manually added.

The list of pioneer transcription factors (pTFs) (Table S5) was compiled from the list published by Lemma et al.[57] in their supplementary Table 4 and Peng et al.[58] in their supplementary Table 5 and 6.

For determination of motifs containing a CpG, power weight matrices (PWM) for all motifs were collected and the CpG score was calculated as follow

For a motif with N positions :

$$CpG\ score = \sum_{i=1}^{N-1} P(C)_i \times P(G)_{i+1} \times (Weight_i + Weight_{i+1})$$

With for each position i,

$$P(C)_i = \frac{Score(C)_i}{Score(A)_i + Score(T)_i + Score(G)_i + Score(C)_i}$$

And

$$Weight_i = \frac{Score(A)_i + Score(T)_i + Score(G)_i + Score(C)_i}{mean(Score_{matrix})}$$

$mean(Score_{matrix})$ being the mean of all the scores present in the position weight matrix.

Then, motifs with a CpG score > 6 were considered as containing at least one CpG.

The P/E score was calculated for each motif as the likelihood that each motif occurrence is present in a promoter rather than an enhancer. For each occurrence of a motif present in a promoter the score is 1, if it is in an enhancer, it is 0. These scores are then averaged over all motif occurrences to give the P/E score of each TF motif.

For k-mean clustering of TF predicted binding scores in wtSRCAP and cdSRCAP treated with IAA or control, TF binding scores were extracted from TOBIAS results for all motifs of the Jaspar2022 database and the Nanog motif. Z-scores were then calculated across samples for each motif and k-mean-clustered using the pheatmap function with a fixed number of 6 clusters.

Motif and Gene Ontology (GO) enrichment

Motif enrichment was performed using the SEA algorithm[114] from the MEME suite using Jaspar non redundant core database as motif database and the default parameters for the other settings. GO enrichment analysis was performed using GOnet[127] with the default parameters and either biological process or molecular function filters for GO terms.

Published datasets

BRG1, Ep400, CHD4 ChIP-Seq raw datasets were obtained from GSE64825 [95]. H3K27ac, H3K4me1, H3K27me3 datasets were obtained from GSE48519 [96]. H2A.Z.1 and H2A.Z.2 ChIP raw datasets were obtained from GSE143737 [20].

Supplemental information

Table S1: Excel file containing RNA-Seq raw counts and differential analysis results

Table S2: Excel file containing results from proteome and chromatome analysis

Table S3: Excel file containing results from TF footprinting analysis

Table S4: List of primers used in the study

Table S5: List of pioneer TFs

Data availability

All sequencing data were deposited at NCBI Gene Expression Omnibus (GEO) under accession number GSEXXXXX.

Proteomics data were deposited at ProteomeXchange under accession number XXXXX.

References

1. Ibarra-Morales, D., Rauer, M., Quarato, P., Rabbani, L., Zenk, F., Schulte-Sasse, M., Cardamone, F., Gomez-Auli, A., Cecere, G., and Iovino, N. (2021). Histone variant H2A.Z regulates zygotic genome activation. Nat Commun *12*, 7002. https://doi.org/10.1038/s41467-021-27125-7.

2. Hickey, G.J., Wike, C.L., Nie, X., Guo, Y., Tan, M., Murphy, P.J., and Cairns, B.R. (2022). Establishment of developmental gene silencing by ordered polycomb complex recruitment in early zebrafish embryos. eLife *11*, e67738. https://doi.org/10.7554/eLife.67738.

3. Liu, X., Zhang, J., Zhou, J., Bu, G., Zhu, W., He, H., Sun, Q., Yu, Z., Xiong, W., Wang, L., et al. (2022). Hierarchical Accumulation of Histone Variant H2A.Z Regulates Transcriptional States and Histone Modifications in Early Mammalian Embryos. Advanced Science *9*, 2200057. https://doi.org/10.1002/advs.202200057.

4. Matsuda, R., Hori, T., Kitamura, H., Takeuchi, K., Fukagawa, T., and Harata, M. (2010). Identification and characterization of the two isoforms of the vertebrate H2A.Z histone variant. Nucleic Acids Research *38*, 4263–4273. https://doi.org/10.1093/nar/gkq171.

5. Hu, G., Cui, K., Northrup, D., Liu, C., Wang, C., Tang, Q., Ge, K., Levens, D., Crane-Robinson, C., and Zhao, K. (2013). H2A.Z Facilitates Access of Active and Repressive Complexes to Chromatin in Embryonic Stem Cell Self-Renewal and Differentiation. Cell Stem Cell *12*, 180–192. https://doi.org/10.1016/j.stem.2012.11.003.

6. Yu, H., Wang, J., Lackford, B., Bennett, B., Li, J., and Hu, G. (2021). INO80 promotes H2A.Z occupancy to regulate cell fate transition in pluripotent stem cells. Nucleic Acids Research *49*, 6739–6755. https://doi.org/10.1093/nar/gkab476.

7. Zhao, B., Chen, Y., Jiang, N., Yang, L., Sun, S., Zhang, Y., Wen, Z., Ray, L., Liu, H., Hou, G., et al. (2019). Znhit1 controls intestinal stem cell maintenance by regulating H2A.Z incorporation. Nat Commun *10*, 1071. https://doi.org/10.1038/s41467-019-09060-w.

8. Wong, M.M., Cox, L.K., and Chrivia, J.C. (2007). The Chromatin Remodeling Protein, SRCAP, Is Critical for Deposition of the Histone Variant H2A.Z at Promoters *. Journal of Biological Chemistry *282*, 26132–26139. https://doi.org/10.1074/jbc.M703418200.

9. Gévry, N., Chan, H.M., Laflamme, L., Livingston, D.M., and Gaudreau, L. (2007). p21 transcription is regulated by differential localization of histone H2A.Z. Genes Dev. *21*, 1869–1881. https://doi.org/10.1101/gad.1545707.

10. Dijkwel, Y., and Tremethick, D.J. (2022). The Role of the Histone Variant H2A.Z in Metazoan Development. Journal of Developmental Biology *10*, 28. https://doi.org/10.3390/jdb10030028.

11. Johnston, H., Kneer, J., Chackalaparampil, I., Yaciuk, P., and Chrivia, J. (1999). Identification of a Novel SNF2/SWI2 Protein Family Member, SRCAP, Which Interacts with CREB-binding Protein*. Journal of Biological Chemistry *274*, 16370–16376. https://doi.org/10.1074/jbc.274.23.16370.

12. Xu, X., Chackalaparampil, I., Monroy, M.A., Cannella, M.T., Pesek, E., Chrivia, J., and Yaciuk, P. (2001). Adenovirus DNA Binding Protein Interacts with the SNF2-Related CBP Activator Protein (SrCap) and Inhibits SrCap-Mediated Transcription. Journal of Virology *75*, 10033–10040. https://doi.org/10.1128/jvi.75.21.10033-10040.2001.

13. Ye, B., Yang, L., Qian, G., Liu, B., Zhu, X., Zhu, P., Ma, J., Xie, W., Li, H., Lu, T., et al. (2020). The chromatin remodeler SRCAP promotes self-renewal of intestinal stem cells. The EMBO Journal *39*, e103786. https://doi.org/10.15252/embj.2019103786.

14. Creyghton, M.P., Markoulaki, S., Levine, S.S., Hanna, J., Lodato, M.A., Sha, K., Young, R.A., Jaenisch, R., and Boyer, L.A. (2008). H2AZ Is Enriched at Polycomb Complex Target Genes in ES Cells and Is Necessary for Lineage Commitment. Cell *135*, 649–661. https://doi.org/10.1016/j.cell.2008.09.056.

15. Ku, M., Jaffe, J.D., Koche, R.P., Rheinbay, E., Endoh, M., Koseki, H., Carr, S.A., and Bernstein, B.E. (2012). H2A.Z landscapes and dual modifications in pluripotent and multipotent stem cells underlie complex genome regulatory functions. Genome Biology *13*, R85. https://doi.org/10.1186/gb-2012-13-10-r85.

16. Murphy, K.E., Meng, F.W., Makowski, C.E., and Murphy, P.J. (2020). Genome-wide chromatin accessibility is restricted by ANP32E. Nat Commun *11*, 5063. https://doi.org/10.1038/s41467-020-18821-x.

17. Berta, D.G., Kuisma, H., Välimäki, N., Räisänen, M., Jäntti, M., Pasanen, A., Karhu, A., Kaukomaa, J., Taira, A., Cajuso, T., et al. (2021). Deficient H2A.Z deposition is

associated with genesis of uterine leiomyoma. Nature *596*, 398–403. https://doi.org/10.1038/s41586-021-03747-1.

18. Rudnizky, S., Khamis, H., Malik, O., Melamed, P., and Kaplan, A. (2019). The base pair-scale diffusion of nucleosomes modulates binding of transcription factors. Proceedings of the National Academy of Sciences *116*, 12161–12166. https://doi.org/10.1073/pnas.1815424116.

19. Pünzeler, S., Link, S., Wagner, G., Keilhauer, E.C., Kronbeck, N., Spitzer, R.M., Leidescher, S., Markaki, Y., Mentele, E., Regnard, C., et al. (2017). Multivalent binding of PWWP2A to H2A.Z regulates mitosis and neural crest differentiation. The EMBO Journal *36*, 2263–2279. https://doi.org/10.15252/embj.201695757.

20. Mylonas, C., Lee, C., Auld, A.L., Cisse, I.I., and Boyer, L.A. (2021). A dual role for H2A.Z.1 in modulating the dynamics of RNA polymerase II initiation and elongation. Nat Struct Mol Biol *28*, 435–442. https://doi.org/10.1038/s41594-021-00589-3.

21. Wen, Z., Zhang, L., Ruan, H., and Li, G. (2020). Histone variant H2A.Z regulates nucleosome unwrapping and CTCF binding in mouse ES cells. Nucleic Acids Research *48*, 5939–5952. https://doi.org/10.1093/nar/gkaa360.

22. Cole, L., Kurscheid, S., Nekrasov, M., Domaschenz, R., Vera, D.L., Dennis, J.H., and Tremethick, D.J. (2021). Multiple roles of H2A.Z in regulating promoter chromatin architecture in human cells. Nat Commun *12*, 2524. https://doi.org/10.1038/s41467-021-22688-x.

23. Lukauskas, S., Tvardovskiy, A., Nguyen, N.V., Stadler, M., Faull, P., Ravnsborg, T., Özdemir Aygenli, B., Dornauer, S., Flynn, H., Lindeboom, R.G.H., et al. (2024). Decoding chromatin states by proteomic profiling of nucleosome readers. Nature *627*, 671–679. https://doi.org/10.1038/s41586-024-07141-5.

24. Shen, T., Ji, F., Wang, Y., Lei, X., Zhang, D., and Jiao, J. (2018). Brain-specific deletion of histone variant H2A.z results in cortical neurogenesis defects and neurodevelopmental disorder. Nucleic Acids Research *46*, 2290–2307. https://doi.org/10.1093/nar/gkx1295.

25. Greenberg, R.S., Long, H.K., Swigut, T., and Wysocka, J. (2019). Single Amino Acid Change Underlies Distinct Roles of H2A.Z Subtypes in Human Syndrome. Cell *178*, 1421-1436.e24. https://doi.org/10.1016/j.cell.2019.08.002.

26. Zilberman, D., Coleman-Derr, D., Ballinger, T., and Henikoff, S. (2008). Histone H2A.Z and DNA methylation are mutually antagonistic chromatin marks. Nature *456*, 125–129. https://doi.org/10.1038/nature07324.

27. Conerly, M.L., Teves, S.S., Diolaiti, D., Ulrich, M., Eisenman, R.N., and Henikoff, S. (2010). Changes in H2A.Z occupancy and DNA methylation during B-cell lymphomagenesis. Genome Res. *20*, 1383–1390. https://doi.org/10.1101/gr.106542.110.

28. Bagchi, D.N., Battenhouse, A.M., Park, D., and Iyer, V.R. (2020). The histone variant H2A.Z in yeast is almost exclusively incorporated into the +1 nucleosome in the direction of transcription. Nucleic Acids Research *48*, 157–170. https://doi.org/10.1093/nar/gkz1075.

29. Bowman, T.A., Wong, M.M., Cox, L.K., Baldassare, J.J., and Chrivia, J.C. (2011). Loss of H2A.Z Is Not Sufficient to Determine Transcriptional Activity of Snf2-Related CBP

Activator Protein or p400 Complexes. International Journal of Cell Biology *2011*, e715642. https://doi.org/10.1155/2011/715642.

30. Nishimura, K., Fukagawa, T., Takisawa, H., Kakimoto, T., and Kanemaki, M. (2009). An auxin-based degron system for the rapid depletion of proteins in nonplant cells. Nat Methods *6*, 917–922. https://doi.org/10.1038/nmeth.1401.

31. Raccaud, M., Friman, E.T., Alber, A.B., Agarwal, H., Deluz, C., Kuhn, T., Gebhardt, J.C.M., and Suter, D.M. (2019). Mitotic chromosome binding predicts transcription factor properties in interphase. Nat Commun *10*, 487. https://doi.org/10.1038/s41467-019-08417-5.

32. King, H.W., and Klose, R.J. (2017). The pioneer factor OCT4 requires the chromatin remodeller BRG1 to support gene regulatory element function in mouse embryonic stem cells. eLife *6*, e22631. https://doi.org/10.7554/eLife.22631.

33. Friman, E.T., Deluz, C., Meireles-Filho, A.C., Govindan, S., Gardeux, V., Deplancke, B., and Suter, D.M. (2019). Dynamic regulation of chromatin accessibility by pluripotency transcription factors across the cell cycle. eLife *8*, e50087. https://doi.org/10.7554/eLife.50087.

34. Niwa, H., Miyazaki, J., and Smith, A.G. (2000). Quantitative expression of Oct-3/4 defines differentiation, dedifferentiation or self-renewal of ES cells. Nat Genet *24*, 372–376. https://doi.org/10.1038/74199.

35. Pundhir, S., Su, J., Tapia, M., Hansen, A.M., Haile, J.S., Hansen, K., and Porse, B.T. (2023). The impact of SWI/SNF and NuRD inactivation on gene expression is tightly coupled with levels of RNA polymerase II occupancy at promoters. Genome Res. *33*, 332–345. https://doi.org/10.1101/gr.277089.122.

36. Ranjan, A., Nguyen, V.Q., Liu, S., Wisniewski, J., Kim, J.M., Tang, X., Mizuguchi, G., Elalaoui, E., Nickels, T.J., Jou, V., et al. (2020). Live-cell single particle imaging reveals the role of RNA polymerase II in histone H2A.Z eviction. eLife *9*, e55667. https://doi.org/10.7554/eLife.55667.

37. Placzek, S., Vanzan, L., and Suter, D.M. (2023). Orchestration of pluripotent stem cell genome reactivation during mitotic exit. Preprint at bioRxiv, https://doi.org/10.1101/2023.08.09.552605 https://doi.org/10.1101/2023.08.09.552605.

38. Kelly, T.K., Miranda, T.B., Liang, G., Berman, B.P., Lin, J.C., Tanay, A., and Jones, P.A. (2010). H2A.Z Maintenance during Mitosis Reveals Nucleosome Shifting on Mitotically Silenced Genes. Molecular Cell *39*, 901–911. https://doi.org/10.1016/j.molcel.2010.08.026.

39. Nekrasov, M., Amrichova, J., Parker, B.J., Soboleva, T.A., Jack, C., Williams, R., Huttley, G.A., and Tremethick, D.J. (2012). Histone H2A.Z inheritance during the cell cycle and its impact on promoter organization and dynamics. Nat Struct Mol Biol *19*, 1076–1083. https://doi.org/10.1038/nsmb.2424.

40. Giaimo, B.D., Ferrante, F., Herchenröther, A., Hake, S.B., and Borggrefe, T. (2019). The histone variant H2A.Z in gene regulation. Epigenetics & Chromatin *12*, 37. https://doi.org/10.1186/s13072-019-0274-9.

41. Palozola, K.C., Donahue, G., Liu, H., Grant, G.R., Becker, J.S., Cote, A., Yu, H., Raj, A., and Zaret, K.S. (2017). Mitotic transcription and waves of gene reactivation during mitotic exit. Science *358*, 119–122. https://doi.org/10.1126/science.aal4671.

42. Yang, Y., Zhang, L., Xiong, C., Chen, J., Wang, L., Wen, Z., Yu, J., Chen, P., Xu, Y., Jin, J., et al. (2022). HIRA complex presets transcriptional potential through coordinating depositions of the histone variants H3.3 and H2A.Z on the poised genes in mESCs. Nucleic Acids Research *50*, 191–206. https://doi.org/10.1093/nar/gkab1221.

43. Gaidatzis, D., Burger, L., Florescu, M., and Stadler, M.B. (2015). Analysis of intronic and exonic reads in RNA-seq data characterizes transcriptional and post-transcriptional regulation. Nat Biotechnol *33*, 722–729. https://doi.org/10.1038/nbt.3269.

44. Blanco, E., González-Ramírez, M., Alcaine-Colet, A., Aranda, S., and Croce, L.D. (2020). The Bivalent Genome: Characterization, Structure, and Regulation. Trends in Genetics *36*, 118–131. https://doi.org/10.1016/j.tig.2019.11.004.

45. Schoenfelder, S., and Fraser, P. (2019). Long-range enhancer–promoter contacts in gene expression control. Nat Rev Genet *20*, 437–455. https://doi.org/10.1038/s41576-019-0128-0.

46. Schneider, J., Wood, A., Lee, J.-S., Schuster, R., Dueker, J., Maguire, C., Swanson, S.K., Florens, L., Washburn, M.P., and Shilatifard, A. (2005). Molecular Regulation of Histone H3 Trimethylation by COMPASS and the Regulation of Gene Expression. Molecular Cell *19*, 849–856. https://doi.org/10.1016/j.molcel.2005.07.024.

47. Policarpi, C., Munafò, M., Tsagkris, S., Carlini, V., and Hackett, J.A. (2024). Systematic epigenome editing captures the context-dependent instructive function of chromatin modifications. Nat Genet, 1–13. https://doi.org/10.1038/s41588-024-01706-w.

48. Wang, H., Fan, Z., Shliaha, P.V., Miele, M., Hendrickson, R.C., Jiang, X., and Helin, K. (2023). H3K4me3 regulates RNA polymerase II promoter-proximal pause-release. Nature *615*, 339–348. https://doi.org/10.1038/s41586-023-05780-8.

49. Willhoft, O., Ghoneim, M., Lin, C.-L., Chua, E.Y.D., Wilkinson, M., Chaban, Y., Ayala, R., McCormack, E.A., Ocloo, L., Rueda, D.S., et al. (2018). Structure and dynamics of the yeast SWR1-nucleosome complex. Science *362*, eaat7716. https://doi.org/10.1126/science.aat7716.

50. Poyton, M.F., Feng, X.A., Ranjan, A., Lei, Q., Wang, F., Zarb, J.S., Louder, R.K., Park, G., Jo, M.H., Ye, J., et al. (2022). Coordinated DNA and histone dynamics drive accurate histone H2A.Z exchange. Science Advances *8*, eabj5509. https://doi.org/10.1126/sciadv.abj5509.

51. Kubik, S., Bruzzone, M.J., Jacquet, P., Falcone, J.-L., Rougemont, J., and Shore, D. (2015). Nucleosome Stability Distinguishes Two Different Promoter Types at All Protein-Coding Genes in Yeast. Molecular Cell *60*, 422–434. https://doi.org/10.1016/j.molcel.2015.10.002.

52. Brahma, S., and Henikoff, S. (2019). RSC-Associated Subnucleosomes Define MNase-Sensitive Promoters in Yeast. Molecular Cell *73*, 238-249.e3. https://doi.org/10.1016/j.molcel.2018.10.046.

53. Jin, C., and Felsenfeld, G. (2007). Nucleosome stability mediated by histone variants H3.3 and H2A.Z. Genes Dev. *21*, 1519–1529. https://doi.org/10.1101/gad.1547707.

54. Jin, C., Zang, C., Wei, G., Cui, K., Peng, W., Zhao, K., and Felsenfeld, G. (2009). H3.3/H2A.Z double variant–containing nucleosomes mark “nucleosome-free regions” of active promoters and other regulatory regions. Nat Genet *41*, 941–945. https://doi.org/10.1038/ng.409.

55. Xi, Y., Yao, J., Chen, R., Li, W., and He, X. (2011). Nucleosome fragility reveals novel functional states of chromatin and poises genes for activation. Genome Res. *21*, 718–724. https://doi.org/10.1101/gr.117101.110.

56. Bentsen, M., Goymann, P., Schultheis, H., Klee, K., Petrova, A., Wiegandt, R., Fust, A., Preussner, J., Kuenne, C., Braun, T., et al. (2020). ATAC-seq footprinting unravels kinetics of transcription factor binding during zygotic genome activation. Nat Commun *11*, 4267. https://doi.org/10.1038/s41467-020-18035-1.

57. Lemma, R.B., Fleischer, T., Martinsen, E., Ledsaak, M., Kristensen, V., Eskeland, R., Gabrielsen, O.S., and Mathelier, A. (2022). Pioneer transcription factors are associated with the modulation of DNA methylation patterns across cancers. Epigenetics & Chromatin *15*, 13. https://doi.org/10.1186/s13072-022-00444-9.

58. Peng, Y., Song, W., Teif, V.B., Ovcharenko, I., Landsman, D., and Panchenko, A.R. (2024). Detection of new pioneer transcription factors as cell-type-specific nucleosome binders. eLife *12*, RP88936. https://doi.org/10.7554/eLife.88936.

59. Ugur, E., de la Porte, A., Qin, W., Bultmann, S., Ivanova, A., Drukker, M., Mann, M., Wierer, M., and Leonhardt, H. (2023). Comprehensive chromatin proteomics resolves functional phases of pluripotency and identifies changes in regulatory components. Nucleic Acids Research *51*, 2671–2690. https://doi.org/10.1093/nar/gkad058.

60. Becker, J.S., McCarthy, R.L., Sidoli, S., Donahue, G., Kaeding, K.E., He, Z., Lin, S., Garcia, B.A., and Zaret, K.S. (2017). Genomic and Proteomic Resolution of Heterochromatin and Its Restriction of Alternate Fate Genes. Molecular Cell *68*, 1023-1037.e15. https://doi.org/10.1016/j.molcel.2017.11.030.

61. Cauchy, P., Koch, F., and Andrau, J.-C. (2017). Two possible modes of pioneering associated with combinations of H2A.Z and p300/CBP at nucleosome-occupied enhancers. Transcription *8*, 179–184. https://doi.org/10.1080/21541264.2017.1291395.

62. Michael, A.K., Grand, R.S., Isbel, L., Cavadini, S., Kozicka, Z., Kempf, G., Bunker, R.D., Schenk, A.D., Graff-Meyer, A., Pathare, G.R., et al. (2020). Mechanisms of OCT4-SOX2 motif readout on nucleosomes. Science *368*, 1460–1465. https://doi.org/10.1126/science.abb0074.

63. Dodonova, S.O., Zhu, F., Dienemann, C., Taipale, J., and Cramer, P. (2020). Nucleosome-bound SOX2 and SOX11 structures elucidate pioneer factor function. Nature *580*, 669–672. https://doi.org/10.1038/s41586-020-2195-y.

64. Masui, S., Nakatake, Y., Toyooka, Y., Shimosato, D., Yagi, R., Takahashi, K., Okochi, H., Okuda, A., Matoba, R., Sharov, A.A., et al. (2007). Pluripotency governed by Sox2 via regulation of Oct3/4 expression in mouse embryonic stem cells. Nat Cell Biol *9*, 625–635. https://doi.org/10.1038/ncb1589.

65. Murphy, P.J., Wu, S.F., James, C.R., Wike, C.L., and Cairns, B.R. (2018). Placeholder Nucleosomes Underlie Germline-to-Embryo DNA Methylation Reprogramming. Cell *172*, 993-1006.e13. https://doi.org/10.1016/j.cell.2018.01.022.

66. Spruijt, C.G., Gnerlich, F., Smits, A.H., Pfaffeneder, T., Jansen, P.W.T.C., Bauer, C., Münzel, M., Wagner, M., Müller, M., Khan, F., et al. (2013). Dynamic Readers for 5-(Hydroxy)Methylcytosine and Its Oxidized Derivatives. Cell *152*, 1146–1159. https://doi.org/10.1016/j.cell.2013.02.004.

67. Domcke, S., Bardet, A.F., Adrian Ginno, P., Hartl, D., Burger, L., and Schübeler, D. (2015). Competition between DNA methylation and transcription factors determines binding of NRF1. Nature *528*, 575–579. https://doi.org/10.1038/nature16462.

68. Azevedo Portilho, N., Saini, D., Hossain, I., Sirois, J., Moraes, C., and Pastor, W.A. (2021). The DNMT1 inhibitor GSK-3484862 mediates global demethylation in murine embryonic stem cells. Epigenetics & Chromatin *14*, 56. https://doi.org/10.1186/s13072-021-00429-0.

69. Kreibich, E., Kleinendorst, R., Barzaghi, G., Kaspar, S., and Krebs, A.R. (2023). Single-molecule footprinting identifies context-dependent regulation of enhancers by DNA methylation. Molecular Cell *83*, 787-802.e9. https://doi.org/10.1016/j.molcel.2023.01.017.

70. McNally, J.G., Müller, W.G., Walker, D., Wolford, R., and Hager, G.L. (2000). The Glucocorticoid Receptor: Rapid Exchange with Regulatory Sites in Living Cells. Science *287*, 1262–1265. https://doi.org/10.1126/science.287.5456.1262.

71. Gebhardt, J.C.M., Suter, D.M., Roy, R., Zhao, Z.W., Chapman, A.R., Basu, S., Maniatis, T., and Xie, X.S. (2013). Single-molecule imaging of transcription factor binding to DNA in live mammalian cells. Nat Methods *10*, 421–426. https://doi.org/10.1038/nmeth.2411.

72. Morisaki, T., Müller, W.G., Golob, N., Mazza, D., and McNally, J.G. (2014). Single-molecule analysis of transcription factor binding at transcription sites in live cells. Nat Commun *5*, 4456. https://doi.org/10.1038/ncomms5456.

73. Schick, S., Grosche, S., Kohl, K.E., Drpic, D., Jaeger, M.G., Marella, N.C., Imrichova, H., Lin, J.-M.G., Hofstätter, G., Schuster, M., et al. (2021). Acute BAF perturbation causes immediate changes in chromatin accessibility. Nat Genet *53*, 269–278. https://doi.org/10.1038/s41588-021-00777-3.

74. Iurlaro, M., Stadler, M.B., Masoni, F., Jagani, Z., Galli, G.G., and Schübeler, D. (2021). Mammalian SWI/SNF continuously restores local accessibility to chromatin. Nat Genet *53*, 279–287. https://doi.org/10.1038/s41588-020-00768-w.

75. Lashgari, A., Millau, J.-F., Jacques, P.-É., and Gaudreau, L. (2017). Global inhibition of transcription causes an increase in histone H2A.Z incorporation within gene bodies. Nucleic Acids Research *45*, 12715–12722. https://doi.org/10.1093/nar/gkx879.

76. Brahma, S., and Henikoff, S. (2024). The BAF chromatin remodeler synergizes with RNA polymerase II and transcription factors to evict nucleosomes. Nat Genet *56*, 100–111. https://doi.org/10.1038/s41588-023-01603-8.

77. Kaur, U., Muñoz, E.N., and Narlikar, G.J. (2024). Hexasomal particles: consequence or also consequential? Current Opinion in Genetics & Development *85*, 102163. https://doi.org/10.1016/j.gde.2024.102163.

78. Dorighi, K.M., Swigut, T., Henriques, T., Bhanu, N.V., Scruggs, B.S., Nady, N., Still, C.D., Garcia, B.A., Adelman, K., and Wysocka, J. (2017). Mll3 and Mll4 Facilitate Enhancer RNA Synthesis and Transcription from Promoters Independently of H3K4

Monomethylation. Molecular Cell *66*, 568-576.e4. https://doi.org/10.1016/j.molcel.2017.04.018.

79. Rickels, R., Herz, H.-M., Sze, C.C., Cao, K., Morgan, M.A., Collings, C.K., Gause, M., Takahashi, Y., Wang, L., Rendleman, E.J., et al. (2017). Histone H3K4 monomethylation catalyzed by Trr and mammalian COMPASS-like proteins at enhancers is dispensable for development and viability. Nat Genet *49*, 1647–1653. https://doi.org/10.1038/ng.3965.

80. Ciabrelli, F., Rabbani, L., Cardamone, F., Zenk, F., Löser, E., Schächtle, M.A., Mazina, M., Loubiere, V., and Iovino, N. (2023). CBP and Gcn5 drive zygotic genome activation independently of their catalytic activity. Science Advances *9*, eadf2687. https://doi.org/10.1126/sciadv.adf2687.

81. Sun, Z.-W., and Allis, C.D. (2002). Ubiquitination of histone H2B regulates H3 methylation and gene silencing in yeast. Nature *418*, 104–108. https://doi.org/10.1038/nature00883.

82. Wu, L., Zee, B.M., Wang, Y., Garcia, B.A., and Dou, Y. (2011). The RING Finger Protein MSL2 in the MOF Complex Is an E3 Ubiquitin Ligase for H2B K34 and Is Involved in Crosstalk with H3 K4 and K79 Methylation. Molecular Cell *43*, 132–144. https://doi.org/10.1016/j.molcel.2011.05.015.

83. Bian, C., Xu, C., Ruan, J., Lee, K.K., Burke, T.L., Tempel, W., Barsyte, D., Li, J., Wu, M., Zhou, B.O., et al. (2011). Sgf29 binds histone H3K4me2/3 and is required for SAGA complex recruitment and histone H3 acetylation. The EMBO Journal *30*, 2829–2842. https://doi.org/10.1038/emboj.2011.193.

84. Cooper, S., Dienstbier, M., Hassan, R., Schermelleh, L., Sharif, J., Blackledge, N.P., De Marco, V., Elderkin, S., Koseki, H., Klose, R., et al. (2014). Targeting Polycomb to Pericentric Heterochromatin in Embryonic Stem Cells Reveals a Role for H2AK119u1 in PRC2 Recruitment. Cell Reports *7*, 1456–1470. https://doi.org/10.1016/j.celrep.2014.04.012.

85. Kalb, R., Latwiel, S., Baymaz, H.I., Jansen, P.W.T.C., Müller, C.W., Vermeulen, M., and Müller, J. (2014). Histone H2A monoubiquitination promotes histone H3 methylation in Polycomb repression. Nat Struct Mol Biol *21*, 569–571. https://doi.org/10.1038/nsmb.2833.

86. Zhao, W., Xu, Y., Wang, Y., Gao, D., King, J., Xu, Y., and Liang, F.-S. (2021). Investigating crosstalk between H3K27 acetylation and H3K4 trimethylation in CRISPR/dCas-based epigenome editing and gene activation. Sci Rep *11*, 15912. https://doi.org/10.1038/s41598-021-95398-5.

87. Chen, C.-W., Zhang, L., Dutta, R., Niroula, A., Miller, P.G., Gibson, C.J., Bick, A.G., Reyes, J.M., Lee, Y.-T., Tovy, A., et al. (2023). SRCAP mutations drive clonal hematopoiesis through epigenetic and DNA repair dysregulation. Cell Stem Cell *30*, 1503-1519.e8. https://doi.org/10.1016/j.stem.2023.09.011.

88. Ding, X., Fan, C., Zhou, J., Zhong, Y., Liu, R., Ren, K., Hu, X., Luo, C., Xiao, S., Wang, Y., et al. (2006). GAS41 interacts with transcription factor AP-2β and stimulates AP-2β-mediated transactivation. Nucleic Acids Research *34*, 2570–2578. https://doi.org/10.1093/nar/gkl319.

89. Gallant, P. (2007). Control of transcription by Pontin and Reptin. Trends in Cell Biology *17*, 187–192. https://doi.org/10.1016/j.tcb.2007.02.005.

90. López-Perrote, A., Alatwi, H.E., Torreira, E., Ismail, A., Ayora, S., Downs, J.A., and Llorca, O. (2014). Structure of Yin Yang 1 Oligomers That Cooperate with RuvBL1-RuvBL2 ATPases *. Journal of Biological Chemistry *289*, 22614–22629. https://doi.org/10.1074/jbc.M114.567040.

91. Wang, Z., Yang, X., Chen, D., Liu, Y., Li, Z., Duan, S., Zhang, Z., Jiang, X., Stockwell, B.R., and Gu, W. (2024). GAS41 modulates ferroptosis by anchoring NRF2 on chromatin. Nat Commun *15*, 2531. https://doi.org/10.1038/s41467-024-46857-w.

92. Feng, Y., Tian, Y., Wu, Z., and Xu, Y. (2018). Cryo-EM structure of human SRCAP complex. Cell Res *28*, 1121–1123. https://doi.org/10.1038/s41422-018-0102-y.

93. Yu, J., Sui, F., Gu, F., Li, W., Yu, Z., Wang, Q., He, S., Wang, L., and Xu, Y. (2024). Structural insights into histone exchange by human SRCAP complex. Cell Discov *10*, 1–18. https://doi.org/10.1038/s41421-023-00640-1.

94. Chen, Z., Gabizon, R., Brown, A.I., Lee, A., Song, A., Díaz-Celis, C., Kaplan, C.D., Koslover, E.F., Yao, T., and Bustamante, C. (2019). High-resolution and high-accuracy topographic and transcriptional maps of the nucleosome barrier. eLife *8*, e48281. https://doi.org/10.7554/eLife.48281.

95. de Dieuleveult, M., Yen, K., Hmitou, I., Depaux, A., Boussouar, F., Dargham, D.B., Jounier, S., Humbertclaude, H., Ribierre, F., Baulard, C., et al. (2016). Genome-wide nucleosome specificity and function of chromatin remodellers in ES cells. Nature *530*, 113–116. https://doi.org/10.1038/nature16505.

96. Hon, G.C., Song, C.-X., Du, T., Jin, F., Selvaraj, S., Lee, A.Y., Yen, C., Ye, Z., Mao, S.-Q., Wang, B.-A., et al. (2014). 5mC Oxidation by Tet2 Modulates Enhancer Activity and Timing of Transcriptome Reprogramming during Differentiation. Molecular Cell *56*, 286–297. https://doi.org/10.1016/j.molcel.2014.08.026.

97. Deluz, C., Friman, E.T., Strebinger, D., Benke, A., Raccaud, M., Callegari, A., Leleu, M., Manley, S., and Suter, D.M. (2016). A role for mitotic bookmarking of SOX2 in pluripotency and differentiation. Genes Dev. *30*, 2538–2550. https://doi.org/10.1101/gad.289256.116.

98. Schindelin, J., Arganda-Carreras, I., Frise, E., Kaynig, V., Longair, M., Pietzsch, T., Preibisch, S., Rueden, C., Saalfeld, S., Schmid, B., et al. (2012). Fiji: an open-source platform for biological-image analysis. Nat Methods *9*, 676–682. https://doi.org/10.1038/nmeth.2019.

99. Dobin, A., Davis, C.A., Schlesinger, F., Drenkow, J., Zaleski, C., Jha, S., Batut, P., Chaisson, M., and Gingeras, T.R. (2013). STAR: ultrafast universal RNA-seq aligner. Bioinformatics *29*, 15–21. https://doi.org/10.1093/bioinformatics/bts635.

100. Zhang, Y., Liu, T., Meyer, C.A., Eeckhoute, J., Johnson, D.S., Bernstein, B.E., Nusbaum, C., Myers, R.M., Brown, M., Li, W., et al. (2008). Model-based Analysis of ChIP-Seq (MACS). Genome Biology *9*, R137. https://doi.org/10.1186/gb-2008-9-9-r137.

101. Ramírez, F., Dündar, F., Diehl, S., Grüning, B.A., and Manke, T. (2014). deepTools: a flexible platform for exploring deep-sequencing data. Nucleic Acids Research *42*, W187–W191. https://doi.org/10.1093/nar/gku365.

102. Neph, S., Kuehn, M.S., Reynolds, A.P., Haugen, E., Thurman, R.E., Johnson, A.K., Rynes, E., Maurano, M.T., Vierstra, J., Thomas, S., et al. (2012). BEDOPS: high-

performance genomic feature operations. Bioinformatics *28*, 1919–1920. https://doi.org/10.1093/bioinformatics/bts277.

103. Quinlan, A.R., and Hall, I.M. (2010). BEDTools: a flexible suite of utilities for comparing genomic features. Bioinformatics *26*, 841–842. https://doi.org/10.1093/bioinformatics/btq033.

104. Li, H., Handsaker, B., Wysoker, A., Fennell, T., Ruan, J., Homer, N., Marth, G., Abecasis, G., Durbin, R., and 1000 Genome Project Data Processing Subgroup (2009). The Sequence Alignment/Map format and SAMtools. Bioinformatics *25*, 2078–2079. https://doi.org/10.1093/bioinformatics/btp352.

105. Chen, K., Xi, Y., Pan, X., Li, Z., Kaestner, K., Tyler, J., Dent, S., He, X., and Li, W. (2013). DANPOS: Dynamic analysis of nucleosome position and occupancy by sequencing. Genome Res. *23*, 341–351. https://doi.org/10.1101/gr.142067.112.

106. Pedersen, B.S., Eyring, K., De, S., Yang, I.V., and Schwartz, D.A. (2014). Fast and accurate alignment of long bisulfite-seq reads. Preprint at arXiv.

107. Akalin, A., Kormaksson, M., Li, S., Garrett-Bakelman, F.E., Figueroa, M.E., Melnick, A., and Mason, C.E. (2012). methylKit: a comprehensive R package for the analysis of genome-wide DNA methylation profiles. Genome Biology *13*, R87. https://doi.org/10.1186/gb-2012-13-10-r87.

108. Love, M.I., Huber, W., and Anders, S. (2014). Moderated estimation of fold change and dispersion for RNA-seq data with DESeq2. Genome Biology *15*, 550. https://doi.org/10.1186/s13059-014-0550-8.

109. Robinson, M.D., McCarthy, D.J., and Smyth, G.K. (2010). edgeR: a Bioconductor package for differential expression analysis of digital gene expression data. Bioinformatics *26*, 139–140. https://doi.org/10.1093/bioinformatics/btp616.

110. Ritchie, M.E., Phipson, B., Wu, D., Hu, Y., Law, C.W., Shi, W., and Smyth, G.K. (2015). limma powers differential expression analyses for RNA-sequencing and microarray studies. Nucleic Acids Research *43*, e47. https://doi.org/10.1093/nar/gkv007.

111. Yu, G., Wang, L.-G., Han, Y., and He, Q.-Y. (2012). clusterProfiler: an R Package for Comparing Biological Themes Among Gene Clusters. OMICS: A Journal of Integrative Biology *16*, 284–287. https://doi.org/10.1089/omi.2011.0118.

112. Wickham, H. (2009). ggplot2: Elegant Graphics for Data Analysis (Springer) https://doi.org/10.1007/978-0-387-98141-3.

113. Durinck, S., Moreau, Y., Kasprzyk, A., Davis, S., De Moor, B., Brazma, A., and Huber, W. (2005). BioMart and Bioconductor: a powerful link between biological databases and microarray data analysis. Bioinformatics *21*, 3439–3440. https://doi.org/10.1093/bioinformatics/bti525.

114. Bailey, T.L., and Grant, C.E. (2021). SEA: Simple Enrichment Analysis of motifs. Preprint at bioRxiv, https://doi.org/10.1101/2021.08.23.457422 https://doi.org/10.1101/2021.08.23.457422.

115. Dull, T., Zufferey, R., Kelly, M., Mandel, R.J., Nguyen, M., Trono, D., and Naldini, L. (1998). A Third-Generation Lentivirus Vector with a Conditional Packaging System. Journal of Virology *72*, 8463–8471. https://doi.org/10.1128/jvi.72.11.8463-8471.1998.

116. Suter, D.M., Cartier, L., Bettiol, E., Tirefort, D., Jaconi, M.E., Dubois-Dauphin, M., and Krause, K.-H. (2006). Rapid Generation of Stable Transgenic Embryonic Stem Cell Lines Using Modular Lentivectors. Stem Cells *24*, 615–623. https://doi.org/10.1634/stemcells.2005-0226.

117. Concordet, J.-P., and Haeussler, M. (2018). CRISPOR: intuitive guide selection for CRISPR/Cas9 genome editing experiments and screens. Nucleic Acids Research *46*, W242–W245. https://doi.org/10.1093/nar/gky354.

118. Egan, B., Yuan, C.-C., Craske, M.L., Labhart, P., Guler, G.D., Arnott, D., Maile, T.M., Busby, J., Henry, C., Kelly, T.K., et al. (2016). An Alternative Approach to ChIP-Seq Normalization Enables Detection of Genome-Wide Changes in Histone H3 Lysine 27 Trimethylation upon EZH2 Inhibition. PLOS ONE *11*, e0166438. https://doi.org/10.1371/journal.pone.0166438.

119. Buenrostro, J.D., Giresi, P.G., Zaba, L.C., Chang, H.Y., and Greenleaf, W.J. (2013). Transposition of native chromatin for fast and sensitive epigenomic profiling of open chromatin, DNA-binding proteins and nucleosome position. Nat Methods *10*, 1213–1218. https://doi.org/10.1038/nmeth.2688.

120. Picelli, S., Björklund, Å.K., Reinius, B., Sagasser, S., Winberg, G., and Sandberg, R. (2014). Tn5 transposase and tagmentation procedures for massively scaled sequencing projects. Genome Res. *24*, 2033–2040. https://doi.org/10.1101/gr.177881.114.

121. Esnault, C., Magat, T., García-Oliver, E., and Andrau, J.-C. (2021). Analyses of PromoterPromoters, Enhancer, and NucleosomeNucleosomesOrganization in Mammalian Cells by MNase-Seq. In Enhancers and Promoters: Methods and Protocols, T. Borggrefe and B. D. Giaimo, eds. (Springer US), pp. 93–104. https://doi.org/10.1007/978-1-0716-1597-3_5.

122. Gao, T., and Qian, J. (2020). EnhancerAtlas 2.0: an updated resource with enhancer annotation in 586 tissue/cell types across nine species. Nucleic Acids Research *48*, D58–D64. https://doi.org/10.1093/nar/gkz980.

123. Lee, S., Zhang, A.Y., Su, S., Ng, A.P., Holik, A.Z., Asselin-Labat, M.-L., Ritchie, M.E., and Law, C.W. (2020). Covering all your bases: incorporating intron signal from RNA-seq data. NAR Genomics and Bioinformatics *2*, lqaa073. https://doi.org/10.1093/nargab/lqaa073.

124. Liao, Y., Smyth, G.K., and Shi, W. (2014). featureCounts: an efficient general purpose program for assigning sequence reads to genomic features. Bioinformatics *30*, 923–930. https://doi.org/10.1093/bioinformatics/btt656.

125. Eisenberg, E., and Levanon, E.Y. (2013). Human housekeeping genes, revisited. Trends in Genetics *29*, 569–574. https://doi.org/10.1016/j.tig.2013.05.010.

126. Castro-Mondragon, J.A., Riudavets-Puig, R., Rauluseviciute, I., Berhanu Lemma, R., Turchi, L., Blanc-Mathieu, R., Lucas, J., Boddie, P., Khan, A., Manosalva Pérez, N., et al. (2022). JASPAR 2022: the 9th release of the open-access database of transcription factor binding profiles. Nucleic Acids Research *50*, D165–D173. https://doi.org/10.1093/nar/gkab1113.

127. Pomaznoy, M., Ha, B., and Peters, B. (2018). GOnet: a tool for interactive Gene Ontology analysis. BMC Bioinformatics *19*, 470. https://doi.org/10.1186/s12859-018-2533-3.

Supplemental figures

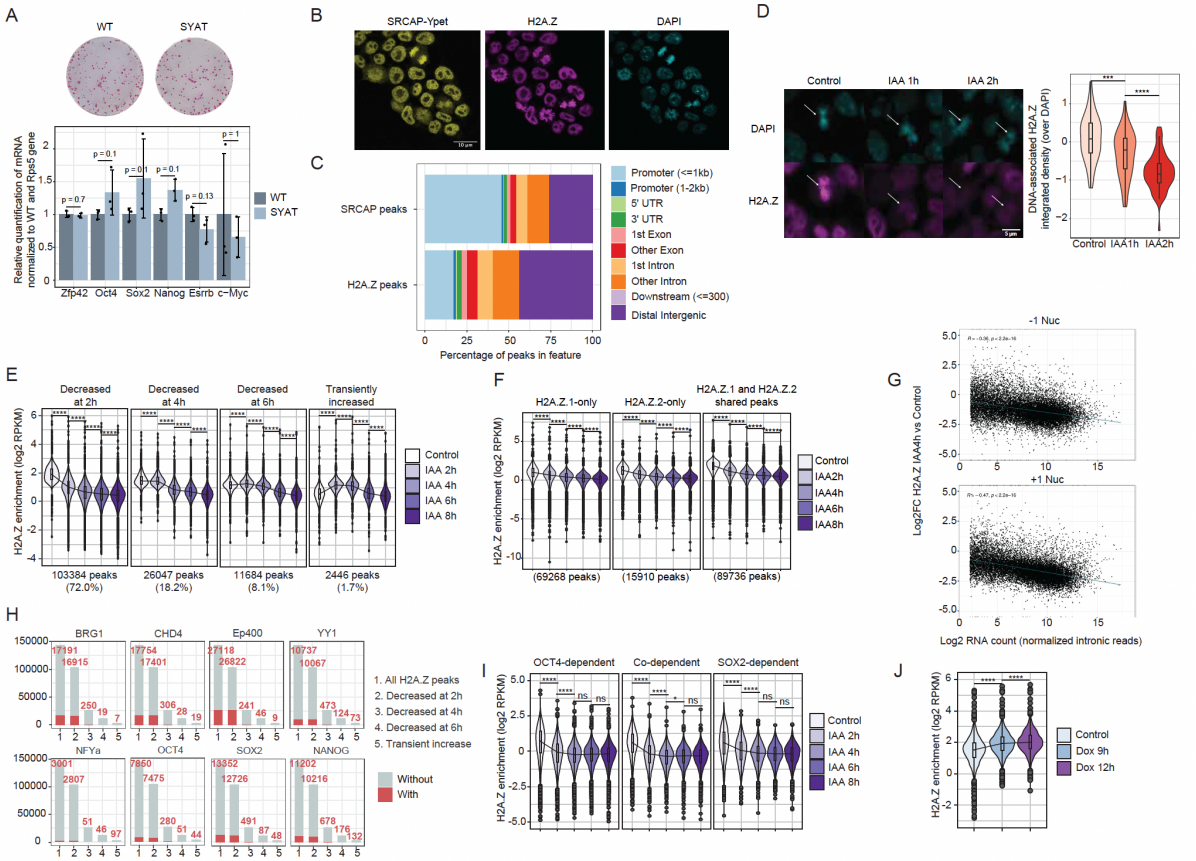

Figure S1. Related to Figure 1. (A) Validation of pluripotency of SYAT cells. Top: Alkaline Phosphatase staining of wt and SYAT mESCs. Bottom: Quantification of pluripotency TF expression by RT-qPCR in wt and SYAT mESCs. N=3. p-values were determined by a Kruskal-Wallis test. (B) Microscopy snapshot of SYAT cells stained with an anti-H2A.Z antibody and DAPI. (C) SRCAP and H2A.Z peak enrichment by genomic locus type. (D) Left: Microscopy snapshots of SYAT cells treated with control or IAA for 2 h and stained with anti-H2A.Z antibody and DAPI. White arrows: mitotic cells. Right: Quantification of DNA-associated H2A.Z normalized on DAPI in mitotic cells treated with IAA or control. N = 50 cells per condition. (E) Classification of H2A.Z-enriched regions as a function of H2A.Z turnover rate. (F) H2A.Z enrichment in SYAT cells treated with control or IAA for 2, 4, 6, or 8 h, at genomic regions enriched for H2A.Z.1, H2A.Z.2 or both. (G) Changes of H2A.Z levels at the -1 and +1 nucleosomes, between 0 and 4 h of IAA treatment, as a function of intronic reads of the downstream genes in the absence of IAA. (H) Total (gray) or enriched (red) peaks for BRG1, CHD4 and Ep400 in the different clusters defined in (D) I. H2A.Z enrichment at regions depending on OCT4 or SOX2 for their accessibility. p-values were determined by a pairwise Wilcoxon test, *: p<0.05, ****: p<0.0001, ns: non-significant. (J) H2A.Z enrichment upon OCT4 knockdown in ZHBTc4 treated with Doxycycline for 9 or 12 h. ****: p<0.0001, *: p<0.05, ns: non-significant. Boxes and outlier points are represented as in Figure 1E.

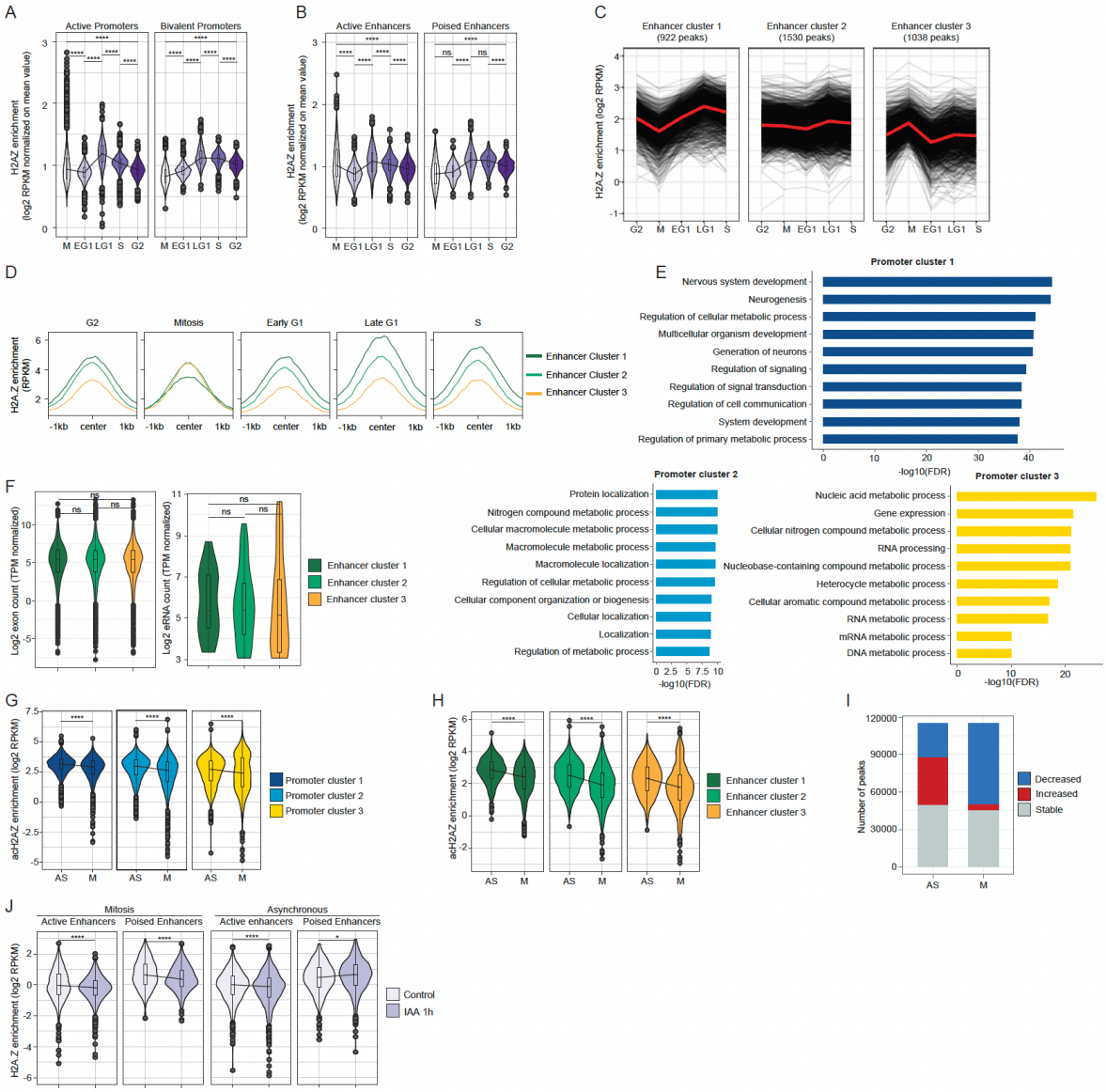

Figure S2. Related to Figure 2. (A) and (B) Mean-normalized scores of each H2A.Z peak calculated from H2A.Z scores across the cell cycle in promoters (A) and enhancers (B). (C) H2A.Z enrichment in enhancer peaks with decreased, stable or increased mitotic H2A.Z levels with respect to G2 and EG1 phases. (D) H2A.Z enrichment around H2A.Z peaks in the clusters defined in (B). (E) Top-ten enriched GO terms in mitotic promoter clusters. (F) Intronic counts of genes regulated by each of the three enhancer clusters (left) and enhancer RNA counts (right) of the enhancers belonging to the three mitotic clusters. (G) and (H) AcH2A.Z enrichment in asynchronous and mitotic cells in mitotic promoter (G) and enhancer (H) clusters. (I) Numbers of peaks displaying increased, stable or decreased H2A.Z score after 1 h of IAA treatment in asynchronous or mitotic cells. (J) H2A.Z enrichment at enhancers in mitotic or asynchronous SYAT cells treated for 1 h with IAA. p-values were determined by a pairwise Wilcoxon test, ****: p<0.0001, ***: p<0.001, **: p<0.01, *: p<0.05, ns: non-significant.

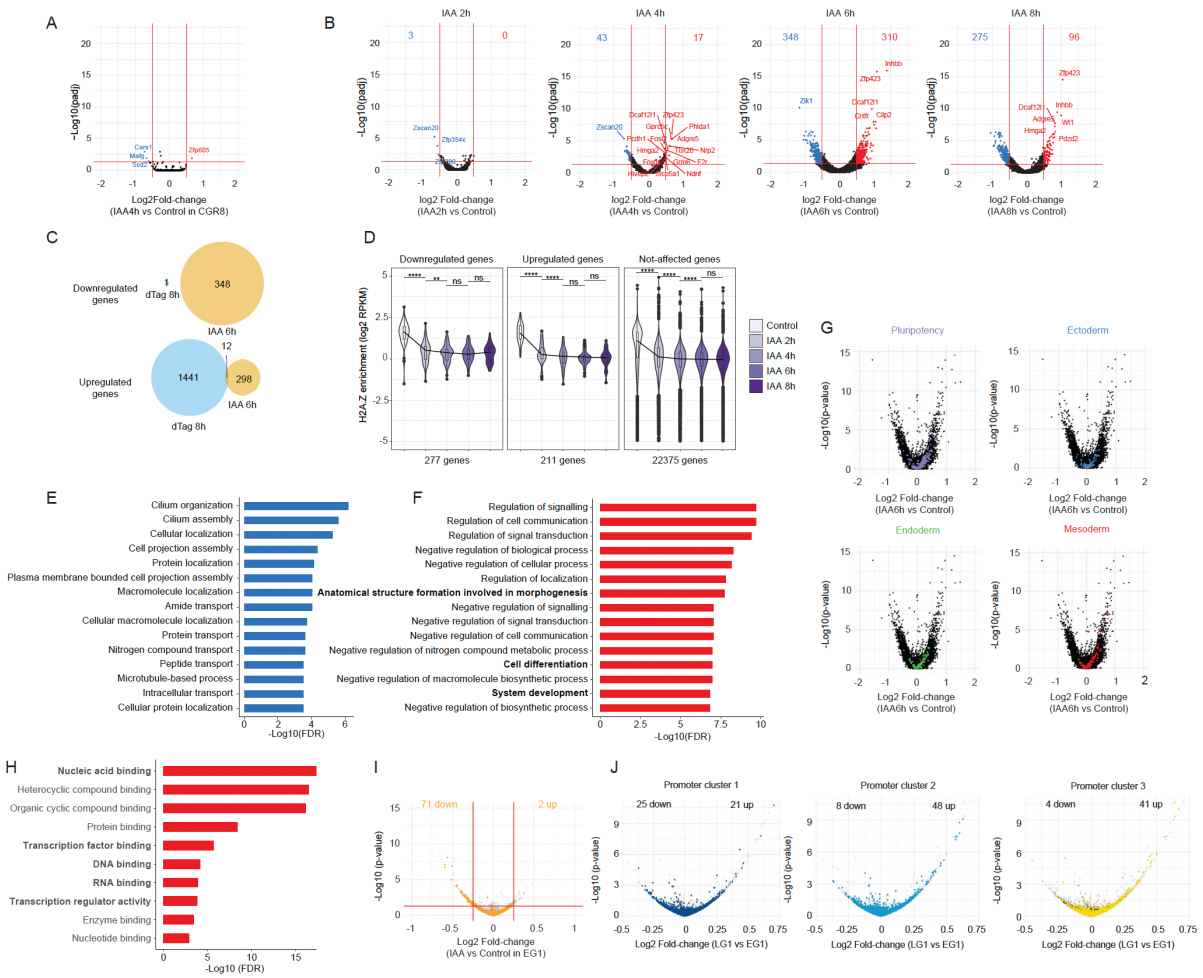

Figure S3. Related to Figure 3. (A) Fold-change of intronic reads and adjusted p-value, for wt cells treated for 4 h with IAA. (B) Fold-change of exonic reads and adjusted p-value, for SYAT cells treated 2, 4, 6 and 8 h with IAA. Numbers: genes significantly downregulated (blue) or upregulated red) with a threshold of |log2FC|>0.5 and adjusted p-value < 0.05. (C) Genes overlapping between those significantly affected after 6 h of IAA treatment and genes affected after 8 h of H2A.Z.1 depletion in [20] when analyzing exonic reads. (D) H2A.Z enrichment (Log2 RPKM) determined by ChIP-Seq, at promoters of upregulated or downregulated genes after 6 h of IAA treatment, or unaffected genes over the course of 8 h of IAA treatment. (E) and (F) Top 15 GO terms enriched for downregulated (E) or upregulated (F) genes after 6 h of IAA treatment in the “cellular process” category. (G) Fold-change of intronic reads and adjusted p-value for SYAT cells treated for 6 h with IAA. Genes associated with pluripotency or commitment to the three germ layers are colored. (H) Top-ten enriched GO terms for molecular functions, in proteins increased in the proteome upon 4 h of IAA treatment. (I) Fold-change of intronic reads for SYAT cells treated for 1 h with IAA and sorted in early G1. Housekeeping genes are colored in orange. Numbers: housekeeping genes significantly downregulated or upregulated with a threshold of |log2FC|>0.25 and p-value < 0.05. p-values were determined by a pairwise Wilcoxon test; ****: p<0.0001; **: p<0.01; ns: non-significant.

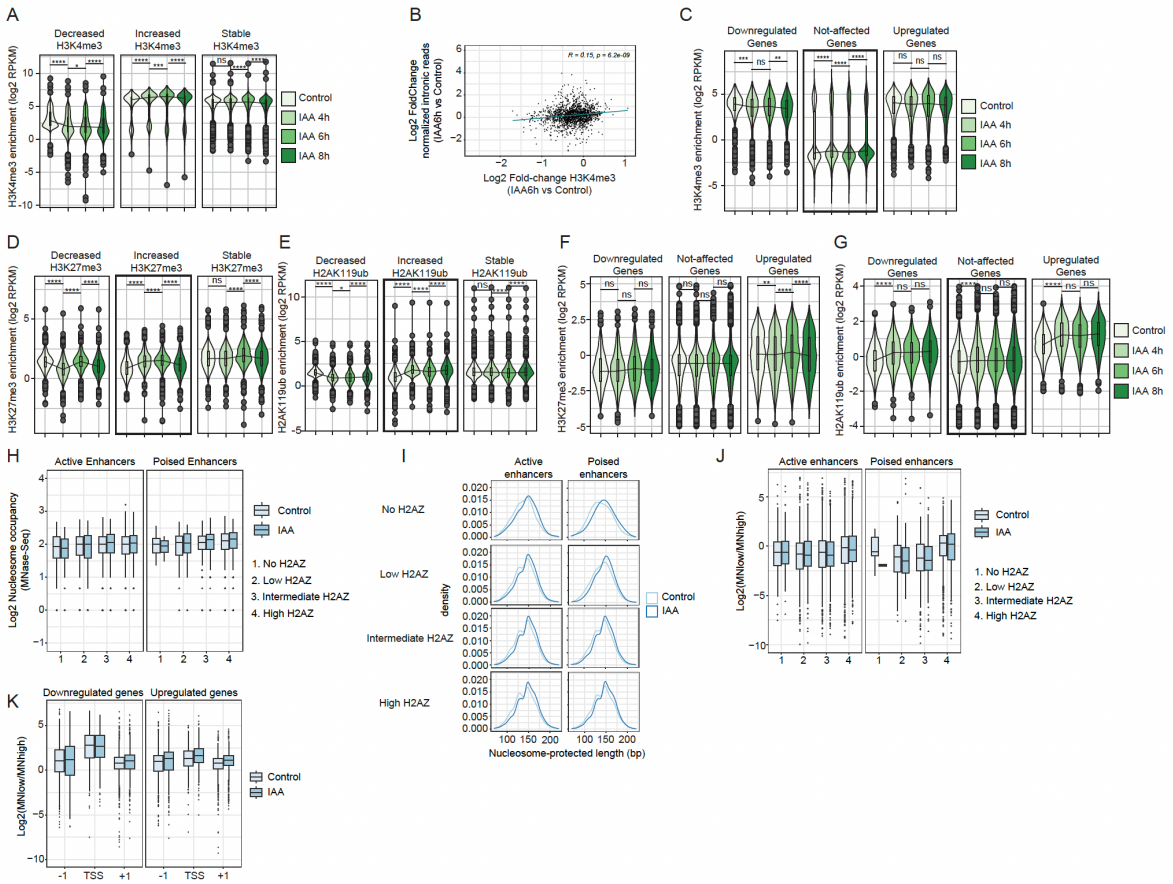

Figure S4. Related to Figure 4. (A) Enrichment of H3K4me3 in SYAT cells treated with control or IAA for 4, 6 and 8 h. (B) Changes in intronic reads of genes controlled by a bivalent promoter as a function of H3K4me3 enrichment between 6 h of IAA treatment and control. Upper right corner: Pearson correlation coefficient. (C) H3K4me3 enrichment in SYAT cells treated with control or IAA for 4, 6 and 8 h, at promoters of genes downregulated or upregulated upon SRCAP depletion. (D) and (E). Enrichment of H3K27me3 (D) and H2AK119ub1 (E) in SYAT cells treated with control or IAA for 4, 6 and 8 h. F and (G) H3K27me3 (F) and H2AK119ub1 (G) enrichment in SYAT cells treated with control or IAA for 4, 6 and 8 h, at promoters of genes downregulated or upregulated upon SRCAP depletion. (H) Nucleosome occupancy at enhancers in SYAT cells as a function of H2A.Z levels, in control or after 4 h of IAA treatment. (I) MNase-Seq fragment densities in SYAT cells treated or not with IAA for 4 h as a function of H2A.Z enrichment and enhancer type. (J) Fragile nucleosomes located at different types of enhancers, as a function of H2A.Z levels. (K) Fragile nucleosomes at -1, TSS and +1 nucleosomes of genes downregulated and upregulated upon SRCAP degradation. p-values were determined by a pairwise Wilcoxon test; ****: p<0.0001; **: p<0.01; *: p<0.05, ns: non-significant.

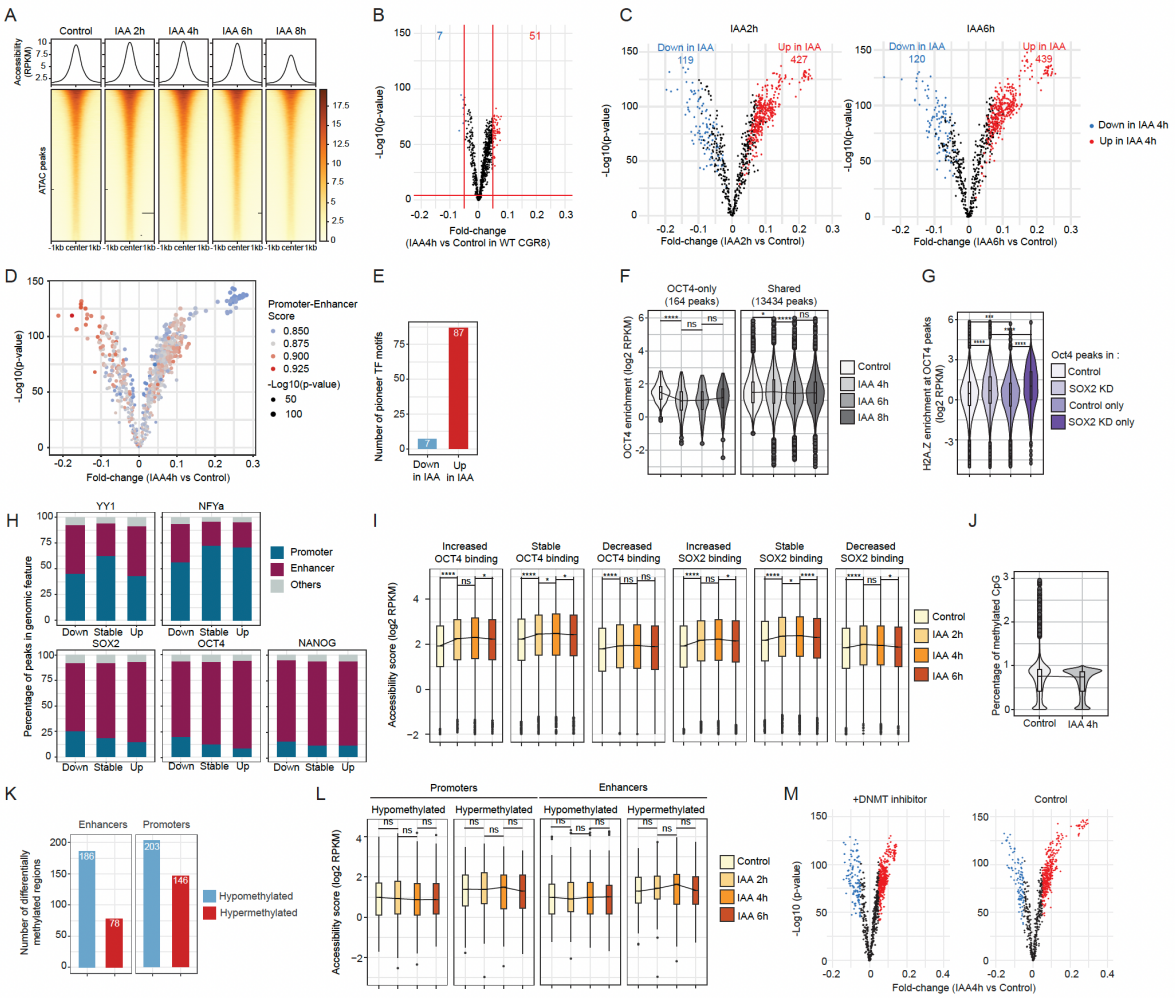

Figure S5. Related to Figure 5. (A) Heatmap of chromatin accessibility determined by ATAC-Seq and centered on the summit of accessible peaks, in SYAT cells upon IAA treatment for 2, 4, 6 and 8 h. (B) Fold-change of TF footprinting calculated using TOBIAS in wt CGR8 cells treated with control or IAA. Colors represent TF motifs predicted to lose (in blue) or gain (in red) binding upon IAA treatment in CGR8 cells with a threshold of |FC|>0.05 and p-value < 0.0001. (C) Fold-change of TF footprinting calculated using TOBIAS in SYAT cells treated 2 h (left panel) or 6 h (right panel) with IAA versus control. Colors: TF motifs predicted to lose (blue) or gain (red) binding upon 4 h-IAA treatment with a threshold of |FC|>0.05 and p-value < 0.0001. (D) Fold-change of TF footprinting calculated using TOBIAS in SYAT cells treated 4 h with IAA versus control. Color scale: promoter-enhancer score; dot size: -log10(p-value). (E) Number of binding motifs of pTFs, among motifs predicted to lose or gain binding upon 4 h of IAA treatment. (F) OCT4 ChIP-seq enrichment score at peaks bound by OCT4 only or shared with SOX2 in SYAT cells treated with IAA for 4, 6 and 8 h or control. (G) H2A.Z enrichment score in 2TS22C cells, at all peaks bound by OCT4 in control conditions, upon SOX2 knockdown, or at peaks unique to control or SOX2 knockdown conditions. (H) Percentage of peaks where TFs increase, decrease or maintain a stable binding upon IAA treatment, in

promoters or enhancers. (I) Accessibility changes upon IAA treatment at peaks gaining, losing or maintaining binding of OCT4 or SOX2. Black line: changes in median values. Boxes: interquartile range, dots: outlier points. (J) Percentage of methylated cytosines in H2A.Z peaks in SYAT cells treated with control or IAA. (K) Number of promoters or enhancers with cytosine hyper- or hypomethylation upon 4 h of IAA treatment. (L) Chromatin accessibility changes upon IAA treatment at hyper- or hypomethylated promoters and enhancers. (M) Fold-change of TF footprinting calculated using TOBIAS, in SYAT cells treated or not for 5 days with a DNMT1 inhibitor and treated 4 h with IAA versus control. p-values were determined by a pairwise Wilcoxon test; ****: $p<0.0001$; ***: $p<0.001$; *: $p<0.05$, ns: non-significant.

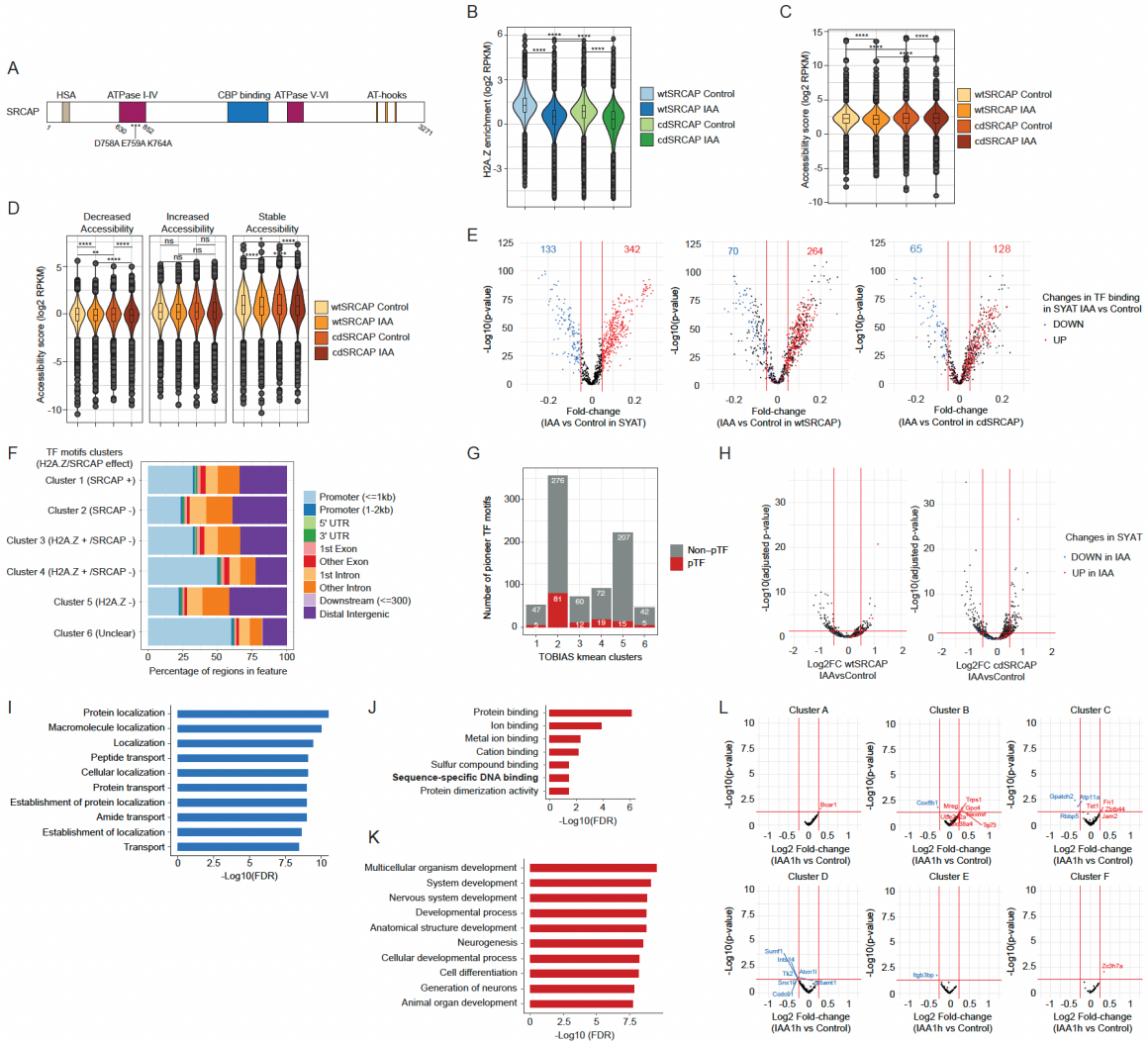

Figure S6. Related to Figure 6. (A) Schematic representation of the SRCAP protein with its functional domains. Stars: mutations introduced in the ATPase domain of SRCAP. (B) H2A.Z enrichment determined by ChIP-Seq in all H2A.Z peaks upon overexpression of wtSRCAP or cdSRCAP and treated with control or IAA for 4 h. (C) Chromatin accessibility changes in all accessible peaks upon overexpression of wtSRCAP or cdSRCAP and treated with control or IAA for 4 h. (D) Chromatin accessibility changes upon overexpression of wtSRCAP or cdSRCAP and treated with control or IAA for 4 h, in peaks gaining, losing, or maintaining accessibility in SYAT cells upon 4 h of IAA treatment. (E) Fold-change of TF footprinting in regions rescued for H2A.Z levels calculated using TOBIAS in SYAT, wtSRCAP and cdSRCAP cells treated with control or IAA for 4 h. Colored dots: motifs predicted to gain or lose binding in rescued regions in SYAT cells treated with IAA versus control. Numbers: Motifs significantly up or down in SYAT and that are still up or down in wtSRCAP or cdSRCAP. (F) Percentage of motif occurrence, belonging to the six clusters determined in Figure 6C, in different types of genomic regions. (G) Number of binding motifs of pioneer TFs in the six motif clusters determined in Fig 6C. (H) Fold-change in intronic reads in

wtSRCAP (left panel) or cdSRCAP (right panel) treated with control or IAA for 4 h. Colors: intronic read changes observed in SYAT cells after 4 h of IAA treatment. (I) Top 10 GO terms in the “cellular process” category, enriched for genes in cluster D and E defined in 6F. (J) Top 10 GO terms in the “molecular function” category, enriched for genes upregulated in cdSRCAP IAA compared to wtSRCAP IAA. (K) Top 10 GO terms in the “cellular process” category, enriched for genes upregulated in cdSRCAP IAA compared to wtSRCAP IAA. (L) Fold-change in intronic reads in the 6 clusters defined in Figure 6F for SYAT cells treated for 1 h with IAA or control and FACSorted in LG1.